Three-body electrodisintegration of the trinucleon system

E. van Meijgaard* and J. A. Tjon
Institute for Theoretical Physics, Princetonplein 5, P.O. Box 80.006, 3508 TA Utrecht, The Netherlands
(Received 21 October 1991)

A theoretical description of the electron-induced three-body breakup process is presented. The continuum wave functions for three outgoing nucleons are determined exactly by solution of the Faddeev equations. A local *s*-wave spin-dependent potential, described by a separable form, is used as two-nucleon input. The response functions of the mirror three-body nuclei are calculated as a function of the energy transfer at momentum transfer values of 300, 400, and 500 MeV/*c*. It is in particular found that the predictions of the longitudinal response function are well in accordance with the experimenal data when the final-state interactions are taken into account.

PACS number(s): 21.45.+v, 25.30.−c, 25.30.Fj

I. INTRODUCTION

In the past decade inclusive and (semi)exclusive inelastic electron scattering experiments on nuclei have provided interesting information about nuclear structure. The weak electromagnetic interaction may be treated perturbatively in very good approximation, which allows a clean separation of the leptonic and hadronic components of the breakup reaction. The theoretical analysis of the nuclear structure is complicated by the presence of nucleonic final-state interactions (FSI), meson-exchange current contributions to the nuclear current (MEC), and the aspect of off-mass shell scattering of the electron on the nucleons in the nuclear bound state. In this respect, the $A=3$ system is especially attractive since for this system the nuclear quantum dynamics can be solved in an exact way, at least in the nonrelativistic regime. Consequently, the effect of FSI on observables related to the breakup reaction can be accounted for properly which enables a much more accurate determination of microscopic properties of the trinucleon bound state, such as the single nucleon momentum distribution.

Recently the nuclear response functions R_L and R_T of the mirror three-body nuclei ^{3}He and ^{3}H have been measured at various values of the momentum-energy transfer [1]. Theoretical predictions in the widely used plane-wave impulse approximation (PWIA) have not been very satisfactory [2,3]. In particular, the longitudinal response functions are generally overestimated by the calculations. The primary objective of this work is to investigate the effect of FSI on the trinucleon response functions.

The calculation of the response functions requires knowledge of the entire spectrum of final states of three nucleons. In addition to the two-body breakup contributions, which are discussed in detail in a previous paper [4,5], we have to know the three-body breakup contributions. In particular, the $3\rightarrow 3$ scattering wave function describing the transition from three off-shell nucleons to three nucleons in the final state is required to determine the electromagnetic three-body breakup amplitude. The construction of such a wave function is discussed in detail with special emphasis on the features in which it differs from the $3N\rightarrow Nd$ scattering wave function needed in the two-body breakup analysis.

Like in the analysis of the two-body breakup process we have taken the local *s*-wave spin-dependent Malfliet-Tjon interaction as N-N input [6]. For technical reasons we adopt a separable approach of this interaction by means of the unitary pole expansion (UPE) [7]. The reproduction of the trinucleon bound-state energy and Nd scattering observables up to 150 MeV in the laboratory system are shown to be quite satisfactory [4]. The actual calculations are mostly done with the first term of the UPE, i.e., the unitary pole approximation (UPA).

The nuclear response functions depend on the momentum-energy transfer and do not contain any information about the nuclear final state. Only the isospin of the nuclear system enters to label the target state. In (semi)exclusive studies some degrees of freedom of the final nuclear state are measured; for example, in a three-body electrodisintegeration experiment one or two of the outgoing nucleons are detected in coincidence with the outgoing electron. Experimentally an exclusive study is significantly more complicated than an inclusive measurement. Only relatively small cross sections are obtained due to the coincidence nature and the weak electromagnetic interaction. Theoretically there are no constraints. Starting with unambiguous amplitudes for the two-body and three-body breakup processes each kinematically complete inelastic process can be calculated. Subsequent summations over unobserved degrees of freedom of the nuclear final state yield (semi)exclusive or inclusive cross sections. At present no kinematically complete experimental data exist for the three-body breakup process. An exception is formed by exclusive ^{3}He$(e,e'p)pn$ data taken at Saclay [8,9]. However, these data are not very useful for an exclusive analysis, since in

*Present address: Royal Netherlands Meteorological Institute, P.O. Box 201, 3730 AE De Bilt, The Netherlands.

fact semi-inclusive data are presented which result from an integration of the exclusive cross sections over the missing energy in order to obtain the three-body breakup momentum distribution of ^{3}He. Furthermore, the second experiment [9] was taken at large missing momentum, such that d waves in the N-N input are needed to explain the results. Therefore, we have selected a number of interesting kinematic situations for which we calculate (semi)exclusive cross sections or related observables, without making an effort to compare the predictions with experimental results.

II. ELECTROMAGNETIC FORMALISM

The unpolarized semi-exclusive $(e,e'N)$ reaction can be expressed in terms of four nuclear structure functions. In the one-photon exchange formalism and treating the electron ultrarelativistically, the cross section takes the form

$$\frac{d^3\sigma}{dE_{e'}d\Omega_{e'}d\mathbf{p}'_N}=\sigma_{\rm Mott}(v_L W_C+v_T W_T+v_S W_S+v_I W_I)\ , \tag{1}$$

where $\sigma_{\rm Mott}=4\alpha^2E_{e'}^2\cos^2(\frac{1}{2}\theta_{e'})/q_\mu^4$, and $\theta_{e'}$ is the scattering angle, $\cos\theta_{e'}=\hat{\mathbf{k}}_{e'}\cdot\hat{\mathbf{k}}_e$ between the incoming and outgoing electron with momenta $\mathbf{k}_e$ and $\mathbf{k}_{e'}$. Information about the nuclear structure is contained in the functions W, while the electron-photon part is described by the functions v. In order to analyze the coincidence cross section in detail we use the frame of reference introduced by de Forest [10]. The orientation of this frame is determined by the momentum transfer $\mathbf{Q}$ and momentum $\mathbf{p}'_N$ of the outgoing nucleon:

$$\begin{aligned}\hat{\mathbf{n}}_z&=\hat{\mathbf{Q}}\ ,\\ \hat{\mathbf{n}}_\perp&=\mathbf{Q}\times\mathbf{p}'_N/|\mathbf{Q}\times\mathbf{p}'_N|\ ,\\ \hat{\mathbf{n}}_\parallel&=\hat{\mathbf{n}}_\perp\times\mathbf{Q}/|\hat{\mathbf{n}}_\perp\times\mathbf{Q}|\ .\end{aligned} \tag{2}$$

In this frame the electron-photon factors v can be written as

$$\begin{aligned}v_L&=(q_\mu/\mathbf{Q}^2)^2\ ,\\ v_T&=\tfrac{1}{2}q_\mu^2/\mathbf{Q}^2+\tan^2\tfrac{1}{2}\theta_{e'}\ ,\\ v_S&=(q_\mu^2/\mathbf{Q}^2)\cos^2\phi+\tan^2\tfrac{1}{2}\theta_{e'}\ ,\\ v_I&=(q_\mu^2/\mathbf{Q}^2)(q_\mu^2/\mathbf{Q}^2+\tan^2\tfrac{1}{2}\theta_{e'})^{1/2}\cos\phi\ ,\end{aligned} \tag{3}$$

where $q_\mu=(\mathbf{Q};i\omega)$ is the four-momentum transfer and ϕ is the angle between the electron plane and the nucleon plane, $\cos\phi=\hat{\mathbf{n}}_\perp\cdot(\mathbf{k}_e\times\mathbf{k}_{e'})/|\mathbf{k}_e\times\mathbf{k}_{e'}|$. The nuclear structure functions W are expressed as products of the various nuclear current components. In shorthand notation we have

$$\begin{aligned}W_C&=\langle\rho_N^2\rangle\ ,\\ W_T&=2\langle J_{N_\perp}^2\rangle\ ,\\ W_S&=\langle J_{N_\parallel}^2\rangle-\langle J_{N_\perp}^2\rangle\ ,\\ W_I&=-\langle\rho_N J_{N_\parallel}\rangle-\langle J_{N_\parallel}\rho_N\rangle\ ,\end{aligned} \tag{4}$$

where conservation of the nuclear current $J_{N_\mu}=(\mathbf{J}_N;i\rho_N)$ is used to eliminate the nuclear current component J_{N_z} in favor of the nuclear charge density:

$$J_{N_z}\rightarrow\frac{\omega}{|\mathbf{Q}|}\rho_N\ . \tag{5}$$

The W functions depend on four kinematic variables, the momentum-energy transfer $Q-\omega$, the outgoing nucleon momentum p_N, and the angle γ between $\mathbf{Q}$ and $\mathbf{p}'_N$. In the adopted frame of reference information about the angle ϕ is factored out and absorbed by the functions v. Apart from the kinematic variables, the W functions also depend on the isospin components T^z of the target nucleus and t_N^z of the detected nucleon.

For the trinucleon system the shorthand notation from Eq. (4) stands for

$$\langle J_{N_\mu}^2\rangle=\frac{1}{2}\sum_{J_T^z}\sum_{f,s_N^z}|^{(-)}\langle\mathbf{p}'_N s_N^z t_N^z,\phi_f f|J_{N_u}|\Psi_T J_T^z T_T^z\rangle|^2 \times\delta(\omega+E_i-E_f)\ , \tag{6}$$

where E_i and E_f are the total energies of the initial and final nuclear systems in the laboratory frame. Furthermore, $|\Psi_T J_T^z T_T^z\rangle$ is the antisymmetrized trinucleon bound state with angular momentum component J_T^z and isopsin component T_T^z, while $|\mathbf{p}'_N s_N^z t_N^z,\phi_f f\rangle^{(-)}$ describes the off-shell scattering of three free nucleons into a final state in which one nucleon has momentum $\mathbf{p}'_N$, spin s_N^z, and isospin t_N^z, while the remaining two nucleons have total momentum $\mathbf{p}=\mathbf{Q}-\mathbf{p}'_N$. The spin-isospin quantum number f together with ϕ_f characterize either a deuteron state or a scattering state.

Our main interest in this work is to determine the three-body breakup nuclear structure functions. Conceptually these functions are closely related to the corresponding two-body breakup contributions, but the three-body breakup process is much harder to deal with in practice due to the continuum spectrum of pair subsystem states $|\phi_f\rangle$. The evaluation of both processes is entirely equivalent with respect to the structure of the electromagnetic nuclear current and the form of the trinucleon bound state, and for a detailed treatment of these aspects we refer to our analysis of the two-body electrodisintegration of ^{3}He.

Once the nuclear structure functions W are known it is straightforward to determine the trinucleon response functions R. They are related to the inclusive scattering cross section according to

$$\frac{d^2\sigma}{dE_{e'}d\Omega_{e'}}=\sigma_{\rm Mott}\left[\frac{q_\mu^4}{\mathbf{Q}^4}R_L+\left[\frac{q_\mu^2}{2\mathbf{Q}^2}+\tan^2\frac{1}{2}\theta_{e'}\right]R_T\right]. \tag{7}$$

Here, R_L and R_T denote, respectively, the longitudinal and transverse response functions. They can in principle be separated experimentally by means of a Rosenbluth plot: For fixed values of Q and ω two measurements are performed at two different electron scattering angles $\theta_{e'}$. It is clear that the response functions are independent of

the final nuclear states, while the isospin of the target nucleus is the only remaining nuclear degree of freedom. The response functions can be expressed in terms of the nuclear structure functions W according to

$$R_L(Q,\omega;T_T^z)=\int d\mathbf{p}'_N W_C \ ,$$
$$R_T(Q,\omega;T_T^z)=\frac{1}{v_T}\int d\mathbf{p}'_N(v_T W_T+v_S W_S) \ , \tag{8}$$

where both the two-body and three-body breakup contributions have to be included in Eq. (8). For the nuclear current we have only considered one-body components, $J_{N_\mu}=\sum_{i=1}^{3} j_{i_\mu}$, for which we have taken an on-mass shell form

$$j_\mu = i[\gamma_\mu(F_1+\kappa F_2)+i(p+p')_\mu \kappa F_2/2M_N] \ . \tag{9}$$

For the electromagnetic form factors F_n we have used those of Höhler *et al.*, set 8.2 [11].

III. THREE-BODY BREAKUP ANALYSIS

A. Three-body final state

The essential difference between two-body breakup and three-body breakup is the treatment of the final state of the pair subsystem. The deuteron state present in the two-body breakup process is an isolated bound state in two-nucleon Hilbert space with a definite internal energy. In the three-body breakup process the pair subsystem is in a continuum state with an internal energy ϵ_{23}, which can vary from the absence of relative motion ($\epsilon_{23}=0$) to absorption of all the relative kinetic energy $s_{\text{c.m.}}$ available in the center-of-mass frame of the three-nucleon system. To determine the three-body breakup amplitude we have to find the solution to the $3N\rightarrow 3N$ scattering process.

Before we discuss these aspects in detail we formulate an explicit expression for the three-body breakup amplitude M from which the nuclear structure function can be calculated. The general form of the amplitude is

$$M_\mu = {}^{A}\langle f|J_{N_\mu}|\Psi_T\rangle \ , \tag{10}$$

where the nuclear states are fully antisymmetric. However, in the actual calculations it is sufficient to consider only one component of the final state $|f\rangle^A$, provided the target state $|\Psi_T\rangle$ is explicitly antisymmetrized and the electromagnetic operator is symmetric in the nucleon labeling. Since $|f\rangle^A$ is constructed by applying the antisymmetrizer A from Eq. (A7) to an unsymmetrized final-state component $|f\rangle$, i.e., $|f\rangle^A=A|f\rangle$, we may as well write

$$M_\mu=\sqrt{6}\langle f|J_{N_\mu}|\Psi_T\rangle \ , \tag{11}$$

where the antisymmetrizer A is absorbed in the target state giving rise to a factor $\sqrt{6}$ due to the asymptotic normalization of $|f\rangle^A$. Of course, $|f\rangle$ still is an eigenstate of the Hamiltonian $H=H_0+\sum_{i=1}^{3}V_i$ at energy $s_{\text{c.m.}}$.

To describe the three-body breakup process we use a complete set of three-particle states in momentum-spin-isospin space. The notation of these states is given in Appendix A. Since the nuclear wave functions are solved with nonrelativistic kinematics, the center-of-mass motion can be taken out from the problem. In terms of the Jacobi momenta $\mathbf{p}_f$ and $\mathbf{q}_f$ the amplitude M_μ can be written as

$$M_\mu(Q,s_{\text{c.m.}};\mathbf{p}_f,\mathbf{q}_f;S_T^z,T_T^z)$$
$$=\sqrt{6}\,{}^{(-)}{}_1\langle \mathbf{p}_f\mathbf{q}_f\beta_f|J_{N_\mu}|\Psi_T S_T^z T_T^z\rangle \ , \tag{12}$$

where β_f represents the spin-isospin quantum numbers according to Eq. (A18).

A kinematically complete, but unpolarized, experiment yields a quantity I which is proportional to the squared amplitude summed over all possible polarizations of the final state. This can be done straightforwardly since the spins in β_f form a complete set. The isospin, however, requires a more careful evaluation, since it does not involve a summation. In a complete experiment we must decide which nucleons are to be detected. Each choice, such that $t_1^z+t_2^z+t_3^z=T^z$, is equivalent, but must remain fixed. It implies that we have to project the isospin states contained in $|\beta_f\rangle$ on the single-nucleon isospin states $|t_1^z t_2^z t_3^z;T^z\rangle$. The corresponding quantity I takes the form

$$I(Q,s_{\text{c.m.}},\mathbf{p}_f,\mathbf{q}_f;t_1^z t_2^z t_3^z,T_T^z)=\delta(H_0(\mathbf{p}_f,\mathbf{q}_f)-s_{\text{c.m.}})$$
$$\times\sum_{s_{p_f},S_f,S_f^z}\frac{1}{2}\sum_{S_T^z}\left|\sum_{t_{p_f},T_f} M_\mu(Q,s_{\text{c.m.}};\mathbf{p}_f,\mathbf{q}_f;S_T^z,T_T^z)\,{}_1\langle(t_{p_f}t_{q_f})T_f T_f^z|t_1^z t_2^z t_3^z\rangle\right|^2 , \tag{13}$$

where

$${}_1\langle(t_{p_f}t_{q_f})T_f T_f^z|t_1^z t_2^z t_3^z\rangle=\langle T_f T_f^z|t_{p_f}t_{p_f}^z t_{q_f}t_{q_f}^z\rangle\langle t_{p_f}t_{p_f}^z|t_2 t_2^z t_3 t_3^z\rangle \ .$$

Throughout the analysis, it is assumed that nucleon 1 is the spectator nucleon, $t_1^z=t_q^z$.

B. Kinematics

The nuclear dynamics related to the construction of the trinucleon wave functions is treated fully nonrelativistically. For reasons of consistency it would be preferable to describe the motion of the three outgoing nucleons by nonrelativistic kinematics as well. However, it turns out that the high end of momentum-energy transfer at which the experimental data are taken requires a theoretical description which goes beyond a purely non-

relativistic treatment. In the analysis of the two-body process [4] relativity is only used to describe the motion of the final N-d state in the laboratory frame and to connect the four-momentum of the transferred photon to the three-momentum of the electromagnetically active nucleon. This procedure was sufficiently accurate to describe the relativistic kinematics of exclusive two-body breakup measurements. In a previous letter [12] we found a significant discrepancy in the positions of the quasielastic peak of the experimental result and the theoretical predictions. The shortcoming certainly had to be ascribed to the use of nonrelativistic kinematics in the description of the three-body breakup process. The discrepancy was resolved by imposing an *ad hoc* method of so-called PWIA kinematics, where the positions of the quasielastic peaks were matched. Hereafter, we will present a more systematic way to connect the relativistic kinematics of the freely moving nucleons with the essentially nonrelativistic momentum arguments of the trinucleon wave functions. The advantage of this prescription is that it not only resolves the above-mentioned discrepancy in a natural way, but it also accounts for the proper relativistic phase space factor of the three-body breakup contribution to the response functions. The latter aspect is described in detail in Appendix B. The results of Sec. IV A show that the use of a relativistic phase space factor leads to significant enhancement of the response functions.

Relativistic kinematics is introduced in the following way. In the center-of-mass frame of the final state of three free nucleons the energy $s_{\rm c.m.}$ is related to a relativistic expression for the kinetic energies $H_0(\mathbf{p}_f,\mathbf{q}_f)$ of the particles according to Eq. (B9). [Use Eq. (A4) to substitute the Jacobi coordinates.] The current matrix elements are calculated in the laboratory and in order to know the final-state momenta $\mathbf{k}_i$ of the nucleons, we apply a Lorentz boost to the c.m.-frame momenta $\mathbf{k}_i^{(\rm c.m.)}$, using the inverse of the transformation in Eq. (B9). In this scheme the energy transfer ω and the center-of-mass energy $s_{\rm c.m.}$ are essentially related by the invariant mass formula,

$$s_{\rm c.m.}+3M_N=\sqrt{(\omega+M_T)^2-\mathbf{Q}^2}\ , \tag{14}$$

where M_T is the mass of the trinucleon bound state. The particle momenta $\mathbf{k}_i^{(in)}$ in the target rest frame are determined from the momenta $\mathbf{k}_i$ in the final state by $\mathbf{k}_i^{(in)}=\mathbf{k}_i-\mathbf{Q}$, $\mathbf{k}_j^{(in)}=\mathbf{k}_j$, and $\mathbf{k}_k^{(in)}=\mathbf{k}_k$, where we have taken particle i as the electromagnetically active nucleon. Since the target rest frame is equivalent to a c.m.-frame, we can directly derive the corresponding Jacobi momenta which are used as input in the determination of the three-nucleon bound-state wave function. This aspect of relativity, which is essential in order to match the positions of the quasielastic peaks, implies a slight modification of the purely nonrelativistic prescription given in Ref. [4] to link Jacobi coordinates of the final and initial states. In fact, it is used in a similar way to calculate the contributions from the two-body breakup process to the response functions.

The last step is to connect the essentially nonrelativistic energy parameter in the three-nucleon final-state wave function with the relativistic energy $s_{\rm c.m.}$, which is related to the energy transfer in the laboratory frame according to Eq. (14). To determine this connection we start from a propagator with relativistic expressions for the energies,

$$G_0^{-1}=H_0(\mathbf{p},\mathbf{q})-s_{\rm c.m.}-i\varepsilon\ . \tag{15}$$

Here we identify the energy $s_{\rm c.m.}$ with the quasielastic point, which is defined by the Jacobi coordinates $\mathbf{p}_f=0$ and $\mathbf{q}_f=\mathbf{q}_{\rm el}$ with $\hat{\mathbf{q}}_{\rm el}\cdot\hat{\mathbf{Q}}=\pm1$, such that

$$s_{\rm c.m.}=\sqrt{\tfrac{4}{3}M_Nq_{\rm el}^2+M_N^2}+2\sqrt{\tfrac{1}{3}M_Nq_{\rm el}^2+M_N^2}\ . \tag{16}$$

An expression for $q_{\rm el}$ as a function of $s_{\rm c.m.}$ is found by associating $q_{\rm el}$ with $q_{\rm max}$ from Eq. (B9).

A nonrelativistic expansion of G_0^{-1} in terms of the off-shell momenta p and q, and the quasielastic momentum $q_{\rm el}$, yields

$$G_0^{-1}=p^2+q^2-q_{\rm el}^2-i\varepsilon\ , \tag{17}$$

which is the nonrelativistic propagator for a system with an effective nonrelativistic energy $\tilde{s}_{\rm c.m.}$ defined by

$$\tilde{s}_{\rm c.m.}=q_{\rm el}^2\ . \tag{18}$$

In the following we will use this effective energy $\tilde{s}_{\rm c.m.}$ as the energy parameter present in the three-particle final-state wave function. Clearly, in a fully nonrelativistic analysis $\tilde{s}_{\rm c.m.}$ is equal to $s_{\rm c.m.}$.

The three-body breakup nuclear structure functions W and the three-body breakup contributions to the nuclear response functions are simply formulated by subsequent integrations over the Jacobi momenta:

$$W(Q,s_{\rm c.m.};\mathbf{q}_f;t_N^z,T_T^z)=\frac{J_1J_2}{n_f}\int d\mathbf{p}_f I(Q,s_{\rm c.m.};\mathbf{p}_f,\mathbf{q}_f;t_1^zt_2^zt_3^z,T_T^z)\ , \tag{19}$$

$$R(Q,s_{\rm c.m.};T_T^z)=\frac{n_f}{2}\int d\mathbf{q}_f W(Q,s_{\rm c.m.};\mathbf{q}_f;t_N^z,T_T^z)\ . \tag{20}$$

The factors J_1 and J_2, together with a phase space factor k_f, which arises when the energy conserving delta function present in the I function is removed by an integration over the length of $\mathbf{p}_f$, are derived in Appendix B.

The factor n_f accounts for the identity of two of the three outgoing nucleons. When the nucleons of the subsystem are identical, $t_2^z=t_3^z$, a factor $\frac{1}{2}$ appears in front of the functions W. Otherwise it appears in front of the response function, reflecting that the spectator nucleon is

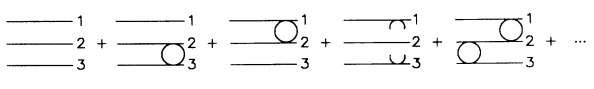

FIG. 1. Diagrammatic representation of the first few terms of the $3N\rightarrow3N$ multiple scattering series.

identical with one of the nucleons in the pair. Thus, the possible values for n_f are

$$n_f=1 \text{ if } t_1^z=+T^z\,, \qquad n_f=2 \text{ if } t_1^z=-T^z\,. \tag{21}$$

C. The scattering wave function

The scattering state corresponding to the transition of three off-shell nucleons to three free nucleons in the final state can be expressed in terms of the three-nucleon T matrix according to

$$|\mathbf{p}_f\mathbf{q}_f\beta_f\rangle_1^{(-)}=|\mathbf{p}_f\mathbf{q}_f\beta_f\rangle_1-\sum_\beta\int d\mathbf{p}\,d\mathbf{q}|\mathbf{pq}\beta\rangle_k G_0(\tilde{s}_{\text{c.m.}})_k\langle\mathbf{pq}\beta|T(\tilde{s}_{\text{c.m.}})|\mathbf{p}_f\mathbf{q}_f\beta_f\rangle_1\,. \tag{22}$$

Here $G_0(z)$ denotes the resolvente operator $(H_0-z)^{-1}$. To determine the free-free T matrix we explicitly make use of the Faddeev equations. Assuming that the potential V is constructed from two-body potentials,

$$V=V_1+V_2+V_3 \tag{23}$$

and decomposing the T matrix as

$$T=T^1+T^2+T^3 \tag{24}$$

the equation for the components T^i can be written as

$$T^i(z)=t_i(z)-t_i(z)G_0(z)[T^j(z)+T^k(z)] \quad (i\neq j\neq k\neq i)\,, \tag{25}$$

where $t_i(z)$ represents the two-body T matrix in the subsystem of particles j and k. With the expression for the Faddeev components $T_i(z)$ we can represent the scattering state of Eq. (22) in diagrammatic form. The first few terms are shown in Fig. 1. The first diagram refers to the pure plane-wave state on the right-hand side of Eq. (22). The next three diagrams each have one nucleon which remains unaffected by FSI. These are called the Born disconnected diagrams and like in the two-body breakup analysis they are treated separately from the fully connected diagrams, of which the last diagram in Fig. 1 is the first representative. The Born disconnected terms can be singled out by applying one iteration to the T matrix of Eq. (22),

$${}_k\langle\mathbf{pq}\beta|T(\tilde{s}_{\text{c.m.}})|\mathbf{p}_f\mathbf{q}_f\beta_f\rangle_1=\sum_{n=1}^{3}{}_k\langle\mathbf{pq}\beta|t_n(\tilde{s}_{\text{c.m.}})|\mathbf{p}_f\mathbf{q}_f\beta_f\rangle_1-\sum_{n=1}^{3}\sum_{l\neq n}{}_k\langle\mathbf{pq}\beta|T^l(\tilde{s}_{\text{c.m.}})G_0(\tilde{s}_{\text{c.m.}})t_n(\tilde{s}_{\text{c.m.}})|\mathbf{p}_f\mathbf{q}_f\beta_f\rangle_1\,. \tag{26}$$

The subindex k in Eq. (22) may be chosen in such a way that it refers to the subsystem where the first nucleonic interaction takes place. However, as is pointed out before, the subindex 1, which labels the final state, must remain fixed, and we need to insert an additional complete set of states in order to recouple to contributions where nucleon 1 is involved in the last nucleonic interaction. In this way the T matrix piece in the second term on the right-hand side of Eq. (22) becomes

$$\begin{aligned}&\sum_\beta\int d\mathbf{p}d\mathbf{q}|\mathbf{pq}\beta\rangle_k\,{}_k\langle\mathbf{pq}\beta|T(\tilde{s}_{\text{c.m.}})|\mathbf{p}_f\mathbf{q}_f\beta_f\rangle_1\\&=\sum_{n=1}^{3}\sum_{\beta'}\int d\mathbf{p}'d\mathbf{q}'\Bigg[\sum_\beta\int d\mathbf{p}\,d\mathbf{q}|\mathbf{pq}\beta\rangle_n\,{}_n\langle\mathbf{pq}\beta|t_n(\tilde{s}_{\text{c.m.}})|\mathbf{p}'\mathbf{q}'\beta'\rangle_n\,{}_n\langle\mathbf{p}'\mathbf{q}'\beta'|\mathbf{p}_f\mathbf{q}_f\beta_f\rangle_1\\&\qquad-\sum_\beta\int d\mathbf{p}\,d\mathbf{q}|\mathbf{pq}\beta\rangle_k\,{}_k\langle\mathbf{pq}\beta|\sum_{l\neq n}T^l(\tilde{s}_{\text{c.m.}})G_0(\tilde{s}_{\text{c.m.}})t_n(\tilde{s}_{\text{c.m.}})|\mathbf{p}'\mathbf{q}'\beta'\rangle_n\,{}_n\langle\mathbf{p}'\mathbf{q}'\beta'|\mathbf{p}_f\mathbf{q}_f\beta_f\rangle_1\Bigg]\,.\end{aligned} \tag{27}$$

The integrals $\int d\mathbf{p}'d\mathbf{q}'$ in Eq. (27) are formal and the momenta $(\mathbf{p}',\mathbf{q}')$ are replaced by the momenta $(\mathbf{p}_{f_n},\mathbf{q}_{f_n})$ associated to the set $(\mathbf{p}_f,\mathbf{q}_f)$ using Appendix A. Furthermore, we must know the spin-isospin recoupling elements ${}_n\langle\beta'|\beta_f\rangle_1$ (see also Appendix A).

The disconnected part of the scattering wave function is calculated straightforwardly. The complications arise in the analysis of the connected part. To determine the multiple scattering series for the $3N\rightarrow 3N$ scattering process we follow the analysis of the related $3N\rightarrow Nd$ scattering process as close as possible [4,13]. The scattering problem of the latter process is solved by iterations of the subsequent scattering terms, starting from the double collision term or rescattering term. For a sufficient number of iterations, in general less than 16, the full solution was determined using the technique of Padé approximants.

To solve the $3N\rightarrow 3N$ scattering problem it turns out that the double collision term is no longer suited to serve as a driving force for the multiple scattering series. This is due to the presence of logarithmic singularities, which are related to the absence of a deuteron state in either the

initial or final state. Fortunately, the triple collision term appears to be sufficiently smooth to act as the starting term for the iterations. Apart from these modifications, the procedures to construct $3N \rightarrow 3N$ and $3N \rightarrow Nd$ scattering series are very similar. The only additional technical problem that remains to be solved is the calculation of the triple collision term. This requires a very careful numerical analysis, which is described in detail in Appendix C.

Once all components are known we can proceed with the calculation of the electromagnetic amplitude M_μ of Eq. (12). As N-N input we have used the local s-wave interactions of Malfliet and Tjon. In both spin-isospin channels it is described by a spin-dependent Yukawa interaction

$$V(r) = -\frac{\lambda_A e^{-\mu_A r}}{r} + \frac{\lambda_R e^{-\mu_R r}}{r} . \tag{28}$$

Like in the study of the two-body breakup process we have employed the UPE to facilitate the numerical evaluations. In this work we have mostly considered only the first term of the UPE series. In momentum space the UPA s-wave matrix element of a local potential is given by

$$V(p,p') = -\lambda g(p) g(p') , \tag{29}$$

where the nucleonic form factor $g(p)$ is the solution of the Lippmann-Schwinger equation which corresponds to the leading eigenvalue. In this approach the two-particle T matrix also separates and takes the analytic form

$$T(\mathbf{p},\mathbf{p}';z) = g(p)\tau(z)g(p') , \tag{30}$$

with

$$\tau(z) = -\left[\lambda^{-1} - 4\pi \int_0^\infty dp\, p^2 \frac{g s p 2(p)}{p^2 - z}\right]^{-1} . \tag{31}$$

A detailed discussion on the validity of the UPE method to N-d scattering and trinucleon bound-state energies can be found in Ref. [4].

D. Electromagnetic amplitude

The various diagrammatic contributions to the electromagnetic amplitude are shown in Fig. 2. The diagrams in Fig. 2(a) represent the process of direct nucleon knockout, while the direct knockout of a correlated pair is contained in Fig. 2(b). The latter diagram is equivalent to the direct deuteron knockout in the two-body breakup process. The diagrams in Figs. 2(c) and 2(d) represent the connected part of the amplitude. It is reminded that each diagram where the photon couples to a nucleon in a correlated pair in fact represents two processes. In addition, the total number of diagrams is three times larger, since the outgoing spectator nucleon can be either nucleon 1, 2, or 3.

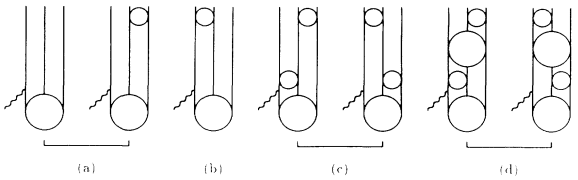

FIG. 2. Diagrammatic representation of the various contributions to the electromagnetic three-body breakup process. Set (a) represents the PWIA-type diagrams, while (b) implies the direct knockout of a correlated pair. The connected diagrams consist of the rescattering contribution given by (c), and all the higher-order diagrams given by (d).

Thus, for a set of six diagrams the probed nucleon is directly knocked into a final plane-wave state. As is well known, the evaluation of these diagrams becomes particularly simple, since the electromagnetic structure can be factorized from nuclear overlap. This set is referred to as the PWIA amplitude, although the convenient way to calculate the PWIA cross section requires an additional assumption.

In the direct amplitude, which is represented by the left-hand diagram in Fig. 2(a), the final state is a pure three-nucleon plane-wave state. Consequently, the calculation of the direct amplitude involves no integrations,

$$M^{(\mathrm{direct})} = \sqrt{6} \langle \psi_T S_T^z T^z | \sum_{n=1}^{3} \Gamma_{\mathrm{e.m.}}^{(n)} | \mathbf{p}_f \mathbf{q}_f \beta_f \rangle_1 . \tag{32}$$

In addition to its simple and fast evaluation, the direct amplitude offers an excellent opportunity to check explicitly whether the numerical representations of the electromagnetic operator and the trinucleon bound state satisfy the symmetry properties required in the derivation of Eq. (12). It should be stressed that this test is important and must be fulfilled, otherwise the numerical results may be senseless. In order to calculate $M^{(\mathrm{direct})}$ a complete set of states $\sum_{\beta'} \int d\mathbf{p}' d\mathbf{q}' |\mathbf{p}'\mathbf{q}'\beta'\rangle_{n\,n} \langle \mathbf{p}'\mathbf{q}'\beta'|$ is inserted in Eq. (32), with the index n taken equal to the active nucleon number n. The desired symmetry test is obtained by inserting the complete set either prior to or after the electromagnetic interaction in Eq. (32). Conceptually, both ways of calculation are completely equivalent and must yield the same result for each set of final-state quantum numbers, regardless of the value of the momentum transfer. In practice, however, the computational schemes are quite different, due to the way the trinucleon bound-state wave function is formulated (see Ref. [4]) and identical results can only be obtained if the symmetry requirements are properly satisfied.

The Born disconnected amplitudes are calculated according to

$$M^{(\mathrm{Born\ discon})} = \sqrt{6} \sum_{n=1}^{3} \sum_{\beta} \int d\mathbf{p}\, d\mathbf{q} \langle \psi_T S_T^z T^z | \sum_{j=1}^{3} \Gamma_{\mathrm{e.m.}}^{(j)} | \mathbf{p}\mathbf{q}\beta \rangle_n G_0(\bar{s}_{\mathrm{c.m.}})_n \langle \mathbf{p}\mathbf{q}\beta | t_n(\bar{s}_{\mathrm{c.m.}}) | \mathbf{p}_f \mathbf{q}_f \beta_f \rangle_1 . \tag{33}$$

The only modification with the two-body breakup analysis is the replacement of the deuteron state by the two-particle t matrix in the continuum sector:

$$\phi_d(\mathbf{p}) \rightarrow \frac{1}{p^2 - p_f^2 - i\varepsilon} t(\mathbf{p}, \mathbf{p}_f; z = p_f^2) \ . \tag{34}$$

The pole in the three-particle propagator is removed using the standard subtraction technique. Of course, the three-body breakup Born amplitudes are complex valued. In contrast to the deuteron case, both spin channels in the two-body sector are accessible. Special care should be attended to the virtual deuteron state in the $^1S_0$ channel just above threshold. The connected amplitude can be written as

$$M^{(\mathrm{con})} = \sqrt{6} \sum_{n=1}^{3} \sum_{\beta} \int d\mathbf{p} d\mathbf{q} \langle \psi_T S_T^z T^z | \sum_{j=1}^{3} \Gamma^{(j)}_{\mathrm{c.m.}} | \mathbf{pq}\beta \rangle_k G_0(\bar{s}_{\mathrm{c.m.}})_k \langle \mathbf{pq}\beta | \sum_{l \neq n} T^l(\bar{s}_{\mathrm{c.m.}}) G_0(\bar{s}_{\mathrm{c.m.}}) t_n(\bar{s}_{\mathrm{c.m.}}) | \mathbf{p}_f \mathbf{q}_f \beta_f \rangle_1 \ , \tag{35}$$

where the index k is chosen in such a way to match the first interacting pair. The wave-function coefficient represents the first rescattering term as well as the account due to the remaining multiple scattering. The structure of these free $\rightarrow$ free scattering terms is analyzed previously and in terms of the corresponding wave functions, the scattering matrix element takes the form

$$\langle \mathbf{pq}\beta | G_0(\bar{s}_{\mathrm{c.m.}}) \sum_{l \neq n} T^l(\bar{s}_{\mathrm{c.m.}}) G_0(\bar{s}_{\mathrm{c.m.}}) t_n(\bar{s}_{\mathrm{c.m.}}) | p_{f_n} q_{f_n} \beta_{f_n} \rangle_n = B^{(1)}(\mathbf{pq}\beta | \mathbf{p}_{f_n} \mathbf{q}_{f_n} \beta_{f_n}) + F(\mathbf{pq}\beta | \mathbf{p}_{f_n} \mathbf{q}_{f_n} \beta_{f_n}) \ . \tag{36}$$

Explicit forms of the functions $B^{(1)}$ and F are expressed in Eqs. (C2) and (C22).

The evaluation of the multiple scattering amplitudes requires a fivefold numerical integration, since the integration of one azimuthal angle can be carried out analytically. This is described in detail in Ref. [4]. An additional complication arises due to the presence of logarithmic singularities in the spectator momentum dependence of the rescattering wave function $B^{(1)}$. In the q integration these poles are removed by means of a subtraction technique. If we construct the function $B^{(1)}$ with the slightly different approach summarized in Eqs. (C20) and (C21), the only logarithmic dependence in the integrand of Eq. (4) is contained in the Q_0 Legendre functions. If we split off a regular coefficient $f(q)$, the integral over the logarithmic contribution can be written as

$$\int_{q_{\omega_1}}^{q_{\omega_2}} dq [f(q) Q_0(x_s(q, q_{f_n})) - 0.5 f(q_{\omega_2}) \ln(q_{\omega_2} - q) + 0.5 k_s f(q_{\omega_1}) \ln(q - q_{\omega_1})] \ , \tag{37}$$

where we have subtracted the singular terms. The position of the logarithmic points q_{ω_1} and q_{ω_2} is known as a function of the associated spectator momentum q_{f_n}

$$\begin{aligned} q_{\omega_1} &= \tfrac{1}{2} | q_{f_n} - \sqrt{3(\bar{s}_{\mathrm{c.m.}} - q_{f_n}^2)} | \ , \\ q_{\omega_2} &= \tfrac{1}{2} [q_{f_n} + \sqrt{3(\bar{s}_{\mathrm{c.m.}} - q_{f_n}^2)}] \ , \end{aligned} \tag{38}$$

where q_{f_n} is related to $\mathbf{p}_f, \mathbf{q}_f$ according to Eq. (A13). [In the notation of Eq. (A13): $j \rightarrow n ; i \rightarrow 1$.] The pole position x_s is expressed in Eq. (C10), the variable k_s corresponds to the sign of x_s at threshold according to Eq. (C10).

The subtraction integrals appearing in Eq. (37) must be compensated, which can be done analytically:

$$\left. \begin{aligned} &\int_{q_{\omega_1}}^{q_{\omega_2}} dq \ln(q_{\omega_2} - q) \\ &\int_{q_{\omega_1}}^{q_{\omega_2}} dq \ln(q - q_{\omega_1}) \end{aligned} \right\} = (q_{\omega_2} - q_{\omega_1})[\ln(q_{\omega_2} - q_{\omega_1}) - 1] \ . \tag{39}$$

In the actual calculation of Eq. (35), the contributions from the rescattering term and the remaining part of the multiple scattering series are separated according to Eq. (36). Except for the account of the logarithmic contributions, which are only present in $B^{(1)}$, the evaluation of both terms is equivalent.

The relative phase between the various amplitudes is of course of importance. Due to the form of the Green's function the real part of subsequent terms in the Faddeev equations [Eq. (5)] have alternating signs. Similarly, the direct amplitude D and the Born disconnected amplitude $B^{(0)}$ have opposite relative sign, which is consistent with Eq. (1). The same is true for $B^{(0)}$ and $B^{(1)}$, respectively, $B^{(1)}$ and F. However, in the latter case the factor -1 is already absorbed in $B^{(2)}$, since the driving term is constructed directly from the expression for $B^{(1)}$.

E. Three-body breakup spectral function

In PWIA it is assumed that the detected nucleon is directly knocked out into a plane-wave state without being affected by the remaining nuclear system. Consequently, the electromagnetic interaction and the complicated overlap of nuclear wave functions factorize, which makes the calculation of the knock-out process significantly simpler.

In order to calculate the breakup observables with PWIA it is customary to introduce the concept of the nu-

clear spectral function. In the discussion of the PWIA-type amplitudes among the various diagrams in Fig. 2 we already mentioned that it is convenient to make one further assumption. In a true PWIA analysis the overlap between contributions with a different active spectator nucleon are neglected. However, the different final states are not orthogonal, which property is expressed by the nonvanishing recoupling coefficients. One consequence of this simplification is that the reduction from a fully antisymmetrized final state to just one component, like in Eqs. (10) and (11), is no longer valid. But we may hope that the overlap contributions are very small compared to the squared terms. In checking this assumption we found that the size of the overlap was indeed very small, less than 1%, which is comparable to the numerical inaccuracy. In this approach the PWIA nuclear structure functions reduce to merely the sum of three equivalent contributions, which contain the spectral function as a factor.

In the three-body breakup process the spectral function measures the probability to find one nucleon t_1^z with missing momentum $\mathbf{q}_m$, leaving the remaining two nucleons in an unbound but correlated state with energy $\varepsilon_{23}(f)=E_m$. Here, we have redefined the missing energy, such that $E_m=0$ indicates the three-body breakup threshold. According to this definition the spectral function can be expressed as

$$S(\mathbf{q}_m,E_m;t_1^z,T_T^z)=\sum_{s_1^z f}\frac{1}{2}\sum_{S_T^z}|\sqrt{3}\langle\psi_T S_T^z T_T^z|\mathbf{q}_m s_1^z;\psi_{23} f\rangle_1|^2\delta(E_m-\varepsilon_{23}(f)) . \tag{40}$$

The correlated two-particle state $|\psi_{23}\rangle$ is antisymmetrized and is assumed to have the same asymptotic normalization as a plane-wave state. The summation index f labels the unobserved quantum numbers of the residual state, i.e., $\sum_f \rightarrow \sum_{s_{23}^z}\int d\mathbf{p}_f$. The energy $\varepsilon_{23}(f)$ is the internal kinetic energy of the subsystem, $\varepsilon_{23}(f)=p_f^2$. Substituting explicit expressions for the trinucleon bound state and the disconnected final states, the spectral function takes the form

$$S(\mathbf{q}_m,E_m;t_1^z,T^z)=\frac{1}{n_f(t_1^z,T^z)}\sum_{s_1^z s_{p_f}}\int d\Omega_{p_f}\left|\sum_{t_{p_f}}\sqrt{6}\left[\psi_T(\mathbf{p}_f,\mathbf{q}_f;\beta_f)-\int d\mathbf{p}\,\psi_T(\mathbf{p},\mathbf{q}_m;\beta_f)\frac{1}{p^2-p_f^2-i\varepsilon}\right.\right.$$
$$\left.\left.\times g(p;\beta_f)\tau(p_f^2;\beta_f)g(p_f;\beta_f)\right]\right.$$
$$\left.\times{}_1\langle((t_{p_f}t_{q_f})T_f T^z|t_1^z t_2^z t_3^z\rangle\right|^2_{p_f=\sqrt{E_m}} , \tag{41}$$

where t_1^z,t_2^z,t_3^z form an arbitrary but fixed set of isospin quantum numbers, such that the isospin factor ${}_1\langle((t_{p_f}t_{q_f})T_f T^z|t_1^z t_2^z t_3^z\rangle$ has a definite value. The factor $\sqrt{6}$ reflects that only one of the six final-state components is used in the actual calculation. The spectral function is normalized in such a way that at fixed values for $\mathbf{q}_m$ and E_m the probabilities to find a nucleon with isospin $t_1^z=T^z$ or $t_1^z=-T^z$ become equal if we assume a spin-independent N-N interaction. The spectral function can be connected to the electromagnetic process by the missing Jacobi coordinate $\mathbf{q}_m$. It is related to the final momentum of the active nucleon according to $\mathbf{q}_m=\frac{1}{2}\sqrt{3/M_N}(\mathbf{Q}-\mathbf{p}'_N)$. In PWIA the nuclear structure functions are simply obtained from

$$W_j^{\mathrm{PWIA}}(Q,\omega,p'_N\gamma;t_1^z,T^z)=\sum_{n=1}^{N_{t_1^z}}\omega_j(Q,\omega,p_N,\gamma;t_1^z)S(\mathbf{q}_m,E_m;t_1^z,T^z) , \tag{42}$$

where the quantities ω_j $(j=C,T,S,I)$ are the corresponding single-nucleon functions. $N_{t_1^z}$ denotes the number of nucleons with isospin t_1^z. The PWIA response functions can be calculated by a subsequent integration over $\mathbf{p}'_N$ according to Eq. (8) or (20).

In PWIA, the missing momentum and missing energy dependence of the three-body part of the spectral function directly determines the three-body breakup nuclear structure properties. To see the form of this dependence we have plotted in Fig. 3 the proton and neutron three-body breakup momentum distribution $\rho_3(\mathbf{p}_m;t_1^z)$ for ^{3}He. This quantity results from an integration of the spectral function over the missing energy in the continuum range,

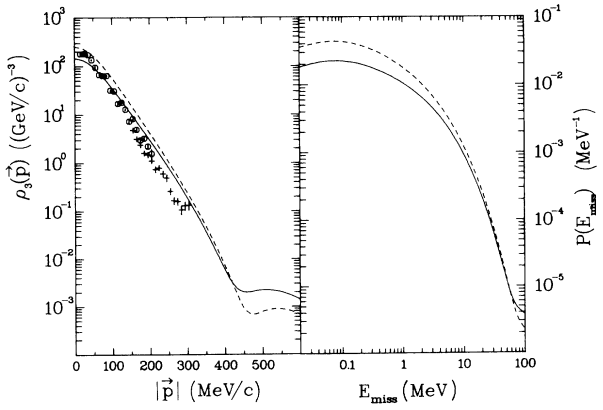

FIG. 3. The left-hand part shows the three-body breakup momentum distribution ρ_3 of ^{3}He calculated in UPA. The figure on the right-hand part shows the function $P(E_m)$, also for ^{3}He. The solid line corresponds to a spectator proton, the dashed line to a spectator neutron.

$$\rho_3(q_m;t_1^z)=\int_0^\infty dE_m S(\mathbf{q}_m,E_m;t_1^z,T^z=\tfrac{1}{2}) \ . \quad (43)$$

Also shown is the less convenient quantity

$$P(E_m;t_1^z)=\frac{1}{4\pi}\int d\mathbf{q}_m S(\mathbf{q}_m,E_m;t_1^z,T^z=\tfrac{1}{2}) \ , \quad (44)$$

from which the missing momentum dependence is removed. The figures clearly show that the spectral function is a rapidly decreasing function of both the missing momentum and missing energy. For more details about the spectral function, such as a two-dimensional plot, the reader is referred to Ref. [2].

Knowledge of the behavior of the spectral function is essential when one wants to calculate the exact nuclear response functions by integrating the squared invariant three-body breakup amplitude $|M|^2$ over the Jacobi coordinates $\mathbf{p}_f$ and $\mathbf{q}_f$. Appendix D provides a detailed description of the integration procedure.

IV. RESULTS

A. Trinucleon response functions

Recently inelastic inclusive cross sections of the mirror nuclei ^{3}He and ^{3}H have been presented by the Bates group [1]. From these measurements the trinucleon response observables are determined as a function of the energy transfer ω in the target rest frame at fixed momentum transfer Q. The experimental data taken at $Q=500$ MeV/c are shown in Figs. 4 and 5. Our theoretical predictions obtained with the use of relativistic kinematics are also shown in Figs. 4 and 5. The energies ω and $s_{\text{c.m.}}$ are linked according to the invariant mass formula from Eq. (14), where we have taken -7.0 MeV for the value of the trinucleon binding energy.

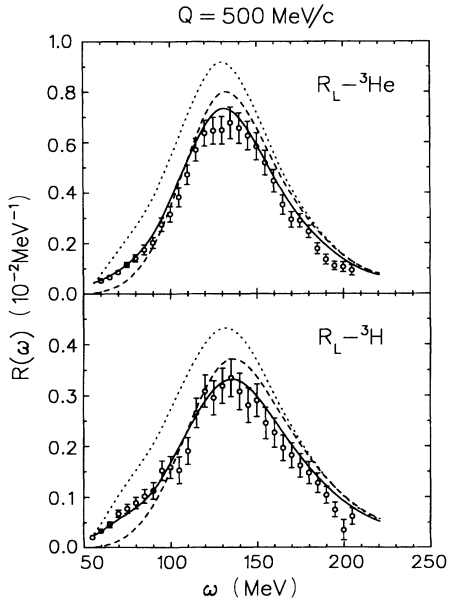

FIG. 4. Longitudinal response functions for ^{3}He and ^{3}H at $Q=500$ MeV/c. The solid curve represents a full calculation. The dashed curve shows the PWIA result, while the dotted curve includes all disconnected contributions. The experimental data are from Ref. [1].

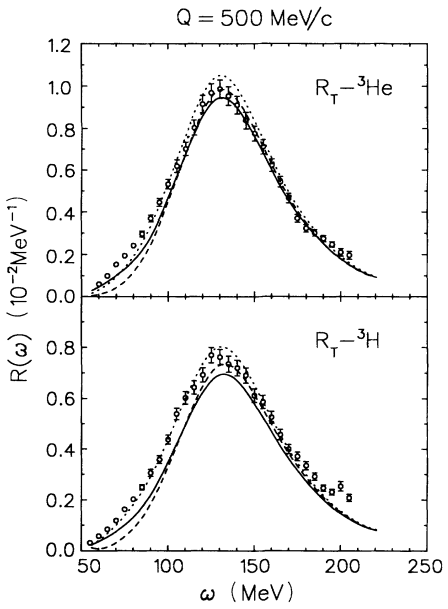

FIG. 5. Transverse response functions for ^{3}He and ^{3}H at $Q=500$ MeV/c. The various curves are the same as in Fig. 4. Data are from Ref. [1].

The full calculation of the longitudinal response turns out to give a reasonable description of the experimental data. The result for the transverse response is less satisfactory. Its prediction underestimates the experimental data throughout the entire quasielastic peak. A possible reason for this discrepancy may be the presence of meson-exchange currents, which will predominantly affect the transverse component of the nuclear current. Another possibility might be the absence of d-wave components in our initial- and final-state wave functions, which is an unlikely cause in view of the PWIA analyses of the Hannover group [2] and the Rome group [3]. In their studies of the response functions with the Reid soft core potential, including d-wave N-N interactions, a similar inadequacy of the calculated transverse response was found.

The figure clearly shows that the addition of the direct knockout of a correlated pair [Fig. 2(b)] to the PWIA contribution [Fig. 2(a)] leads to a significant enhancement of the response functions. However, this effect is entirely canceled by the addition of the connected amplitudes of Figs. 2(c) and 2(d). In fact, the inclusion of FSI results in a sizable reduction of the response relative to PWIA for values of the energy transfer throughout the quasielastic peak. Only at low energy transfer final-state effects tend to increase the PWIA response, while at energy transfer values beyond $\omega=200$ MeV the effect on the response functions becomes negligible.

This result does not support the findings of Schiavilla *et al.* [14], who used the method of correlated basis states to account for some final-state effects. The entire response peak in their full result is shifted towards larger

energies with respect to the result obtained in impulse approximation (IA). Consequently, the full response is enhancing the IA response at energies beyond the quasielastic peak, despite the fact that the strength of the peak is decreased by about 15%. It should be noted, however, that their uncorrelated result in principle corresponds to only the first diagram of Fig. 2.

To see the effect of relativistic kinematics as described in Sec. III B and Appendix B, we have also calculated the response using purely nonrelativistic kinematics. Results for the longitudinal response obtained with both kinematics are shown in Fig. 6. The effect of relativistic kinematics is clearly visible, both to the size of the response functions and to the position of the quasielastic peak. The enhancement found is entirely due to the relativistic phase space factor. The shift of the quasielastic peak to lower values of the energy transfer is primarily induced by the way the relativistic nucleon momenta of the final state is linked with the nonrelativistic nuclear dynamics of the trinucleon wave functions as has been described in Sec. III B.

The top of the quasielastic peak is roughly located at the point where the energy transfer satisfies the relation

$$\omega + M_T = \sqrt{Q^2 + M_n^2} + 2M_N \ . \tag{45}$$

This point corresponds to a kinematic situation where all nucleons are at rest prior to the e.m. knockout, such that the nuclear spectral function gives a maximal contribution. Using relativistic kinematics this point is found at $\omega = 131.6$ MeV, whereas in the nonrelativistic approach the top shifts to $\omega = 140.2$ MeV. Still, the response functions obtained with relativistic kinematics appear to be slightly to the right of the above-mentioned figure. This is due to the fact that the phase space factor is a rising function of the energy transfer. In Fig. 6 only the effect of relativity to the full results is shown. It turns out that in going to relativistic kinematics the various approximations show a similar shift and enhancement, such that the relative shapes and positions of all calculated results remain the same in both kinematics. This is of course not surprising, since in both kinematics the nuclear dynamics, in which the full result and its approximations differ, is treated nonrelativistically.

In Refs. [4] and [5] it is verified that use of the unitary pole approximation (UPA), i.e., the first term of the unitary pole expansion (UPE) series, leads to realistic results in the calculation of exclusive two-body breakup cross sections. It is important to establish whether such a statement holds in the analysis of three-body breakup processes and hence in the calculation of the response functions. We have therefore studied the sensitivity of the nuclear response functions on the number of eigenvalues retained in the UPE series. Using the notation of Ref. [4] the results for the ^{3}He longitudinal response function obtained with UPA, (1111)-UPE, and (2222)-UPE are listed in Table I. The ratio of (2222)-UPE results and the UPA results for the various response functions are tabulated in Table II. In this notation UPA is equivalent to (1010)-UPE. In Ref. [4] it is found that the observables calculated with a (2222)-UPE analysis, i.e., with four terms in each two-nucleon channel, have almost converged to the same value obtained with a calculation based on the corresponding local potential. So keeping even more eigenvalues is not necessary. We have selected three kinematic points, one on the high-energy transfer side of the response (kinematics I), another point at the top of the quasielastic peak (kinematics II), and a

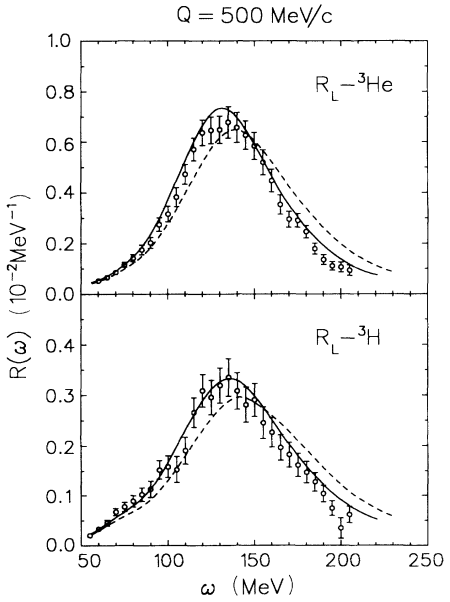

FIG. 6. Longitudinal response functions for ^{3}He and ^{3}H at $Q = 500$ MeV/c obtained with relativistic and nonrelativistic kinematics. The relativistic result is represented by the solid curve, which is the same as in Fig. 4. The dashed curve shows the full result obtained with the use of purely nonrelativistic kinematics. Data are from Ref. [1].

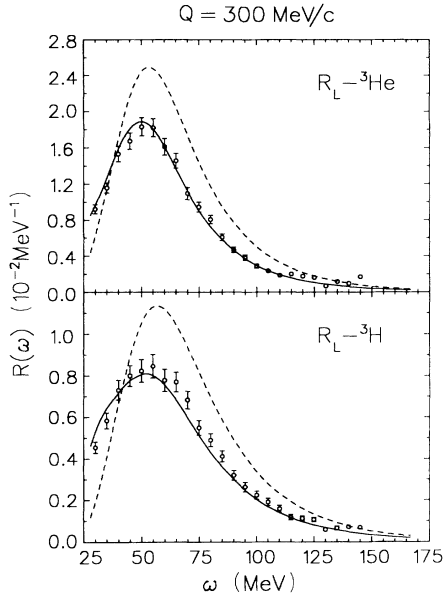

FIG. 7. Longitudinal response functions for ^{3}He and ^{3}H at $Q = 300$ MeV/c. The various curves are the same as in Fig. 4. Data are from Ref. [1].

TABLE I. Longitudinal response function of ^{3}He (in units of 10^{-2} MeV^{-1}) at three kinematic points obtained with a UPA and with two high-term UPE calculations. Apart from the response function we have also listed two-body breakup and the three-body breakup contributions to the response function separately. We have tabulated the results of a PWIA calculation together with the results of a full analysis including FSI.

	Two-body breakup		Three-body breakup		Total breakup	
R_L-^{3}He	PWIA	+FSI	PWIA	+FSI	PWIA	+FSI
	Kinematics I: $Q=300$ MeV/c, $s_{\text{c.m.}}=80$ MeV, $\omega=100.9$ MeV					
UPA	0.2595	0.1520	0.2279	0.1390	0.4874	0.2909
(1111)-UPE	0.2476	0.1514	0.2201	0.1366	0.4677	0.2880
(2222)-UPE	0.2466	0.1461	0.2198	0.1353	0.4664	0.2815
	Kinematics II: $Q=500$ MeV/c, $s_{\text{c.m.}}=80$ MeV, $\omega=128.3$ MeV					
UPA	0.5702	0.5257	0.2232	0.2057	0.7934	0.7314
(1111)-UPE	0.5872	0.5392	0.2241	0.2034	0.8113	0.7426
(2222)-UPE	0.5876	0.5430	0.2241	0.2100	0.8116	0.7530
	Kinematics III: $Q=500$ MeV/c, $s_{\text{c.m.}}=20$ MeV, $\omega=70.7$ MeV					
UPA	0.0240	0.0592	0.0098	0.0346	0.0338	0.0938
(1111)-UPE	0.0222	0.0549	0.0091	0.0315	0.0313	0.0863
(2222)-UPE	0.0220	0.0568	0.0091	0.0338	0.0312	0.0906

point on the low-energy transfer side of the response curve (kinematics III). Table II shows that the response function results obtained with a full analysis including FSI with either UPA or (2222)-UPE do not differ more than about 3%, except for the transverse response functions in kinematics III which differ around 5%. Furthermore, the (2222)-UPE response curves have a larger maximum and are steeper than the UPA response curves. The differences in the PWIA calculations are a bit larger, with the overall effect that changing from UPA to (2222)-UPE tends to lift the curve corresponding to a full calculation relative to the PWIA result by a few percent. However, this is a very small effect, and comparison of the numbers listed in the last two columns of Table I shows that the role of final state interactions remains almost unaffected in turning from UPA to (2222)-UPE. In view of these aspects we conclude that it is indeed justified to consider UPA as a very useful tool in the analysis of the three-body response observable. The results for the two-body breakup and three-body breakup contributions to the response function are listed separately, showing that neither one nor the other breakup pro-

TABLE II. Ratio values of the response functions obtained with a high-term (2222)-UPE calculation and with a UPA calculation at three kinematic points. Remaining details are explained in the caption of Table I.

	Two-body breakup		Three-body breakup		Total breakup	
	PWIA	+FSI	PWIA	+FSI	PWIA	+FSI
	Kinematics I: $Q=300$ MeV/c, $s_{\text{c.m.}}=80$ MeV, $\omega=100.9$ MeV					
R_L-^{3}He	0.951	0.962	0.964	0.974	0.957	0.967
R_L-^{3}H	0.930	1.068	0.978	0.969	0.978	0.971
R_T-^{3}He	0.948	0.941	0.969	1.000	0.960	0.978
R_T-^{3}H	0.950	0.936	0.974	0.995	0.969	0.983
	Kinematics II: $Q=500$ MeV/c, $s_{\text{c.m.}}=80$ MeV, $\omega=128.3$ MeV					
R_L-^{3}He	1.034	1.033	1.004	1.021	1.023	1.030
R_L-^{3}H	1.019	1.060	1.016	1.025	1.016	1.026
R_T-^{3}He	1.030	1.031	1.008	1.024	1.021	1.028
R_T-^{3}H	1.030	1.030	1.013	1.021	1.019	1.025
	Kinematics III: $Q=500$ MeV/c, $s_{\text{c.m.}}=20$ MeV, $\omega=70.7$ MeV					
R_L-^{3}He	0.918	0.961	0.935	0.977	0.923	0.967
R_L-^{3}H	0.912	1.037	0.948	1.016	0.947	1.026
R_T-^{3}He	0.919	0.951	0.940	0.938	0.927	0.946
R_T-^{3}H	0.919	0.949	0.945	0.950	0.935	0.949

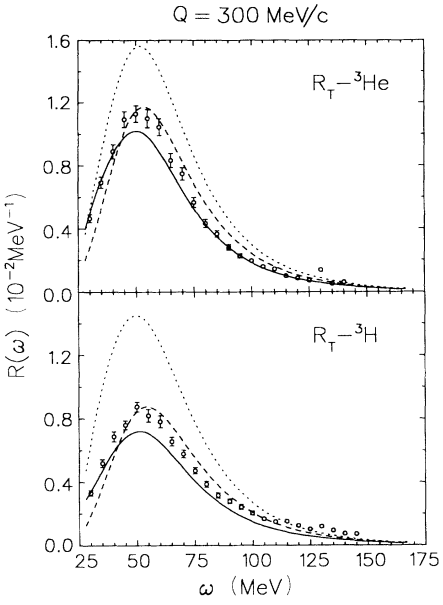

FIG. 8. Transverse response functions for ^{3}He and ^{3}H at $Q=300$ MeV/c. The various curves are the same as in Fig. 4. Data are from Ref. [1].

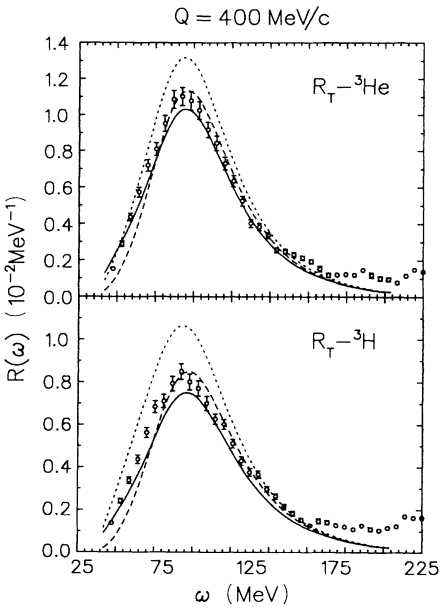

FIG. 10. Transverse response functions for ^{3}He and ^{3}H at $Q=400$ MeV/c. The various curves are the same as in Fig. 4. Data are from Ref. [1].

cess is particularly sensitive to the number of eigenvalues retained in the UPE series. With a few exceptions, the (1111)-UPE results are between the UPA and (2222)-UPE results.

The calculation of the response functions has also been done at a momentum transfer of 300 and 400 MeV/c. The results are shown in Figs. 7–10, together with the experimental data from Bates [1]. Again relativistic kinematics is employed. In view of the lower momentum transfer, however, the effect of relativity is smaller than found in Fig. 6. Similarly to the previous analysis the description of the longitudinal data appears to be quite

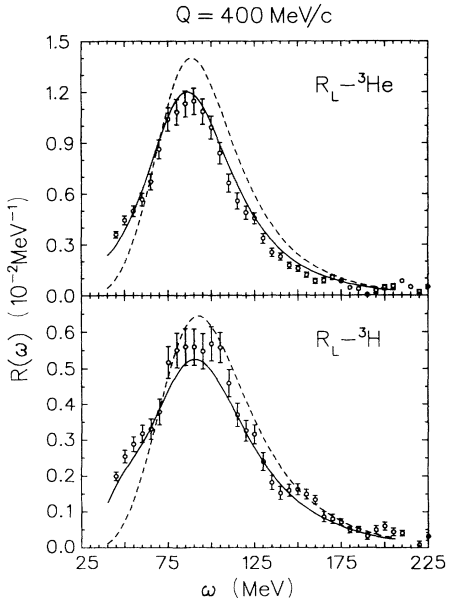

FIG. 9. Longitudinal response functions for ^{3}He and ^{3}H at $Q=400$ MeV/c. The various curves are the same as in Fig. 4. Data are from Ref. [1].

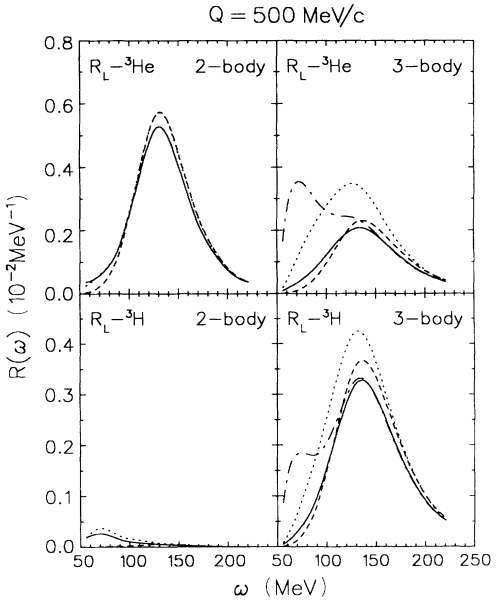

FIG. 11. Two-body and three-body breakup contributions to the longitudinal response of ^{3}He and ^{3}H separately at $Q=500$ MeV/c. The solid curve represents a full calculation. The dashed curve shows the PWIA result, while the dotted curve includes all disconnected contributions. The dash-dotted curve in the figures corresponding to the three-body breakup contribution indicates a calculation including all disconnected amplitudes and the lowest-order connected amplitudes.

reasonable. In particular, the ^{3}He data are accurately reproduced. However, the calculated tranverse response falls again well below the experimental data.

It is interesting to see the two-body and three-body breakup to the response functions separately. They are shown in Figs. 11 and 12 for the longitudinal response only. A number of features are worth mentioning. The ^{3}H longitudinal response is entirely determined by the three-body breakup part. The two-body breakup PWIA contribution to this response function is negligible. However, it turns out that final-state interactions do not affect this result significantly, except for low values of the energy transfer. Furthermore, the two-body breakup disconnected contribution is almost completely determined by the PWIA amplitude. Although direct deuteron knockout is the dominant process in antiparallel kinematics [4], the PWIA peak in forward direction is generally much more pronounced. A similar behavior of the various disconnected amplitudes is found in the three-body breakup process. However, as both figures clearly show, the Born disconnected contribution to the response is considerably enhanced relative to the PWIA contribution. This can be partly ascribed to the enlarged accessible phase space for three outgoing particles compared to the two-body breakup process. There are three PWIA related peaks, which are very narrow like in the two-body breakup process. The gamma-correlated-pair contribution, however, is more spread than its two-body breakup counterpart. Another effect is the nonvanishing overlap between the three nonorthogonal final-state components. It turns out that in a calculation with only disconnected amplitudes these interference terms amount for 10% to 20% of the response.

Final-state effects always decrease the disconnected response. For the three-body breakup process, shown in the right-hand side of Figs. 11 and 12, we have plotted a curve, which results after truncating the scattering series at the first rescattering term. For all energies, the disconnected result is considerably affected by the addition of the rescattering term, and it is evidently wrong to ignore the lowest-order connected diagrams. At low energies, however, the truncation of the diagrammatic series at the rescattering term leads to a striking enhancement of the response. In this energy domain one is forced to include the remaining terms of the multiple scattering series in order to describe the experimental data reasonably. In particular, for the case of the low momentum transfer the addition of the remaining multiple scattering effects has dramatic consequences for the approximate response up to the order of the rescattering contribution. At increasing energy transfer the difference between the full result and the result up to first-order connected diagrams is gradually decreasing. For the $Q=500$ MeV/c kinematics the difference becomes less than 1% beyond $\omega=175$ MeV; however, for the $Q=300$ MeV/c kinematics the difference is still 10% at this value of ω. Similar figures can be drawn for the tranverse response; however, the effect of final-state interactions to the PWIA and Born results is much smaller than it is for the case of the longitudinal response, which can already be seen in Figs. 4 and 5, respectively, Figs. 7 and 8.

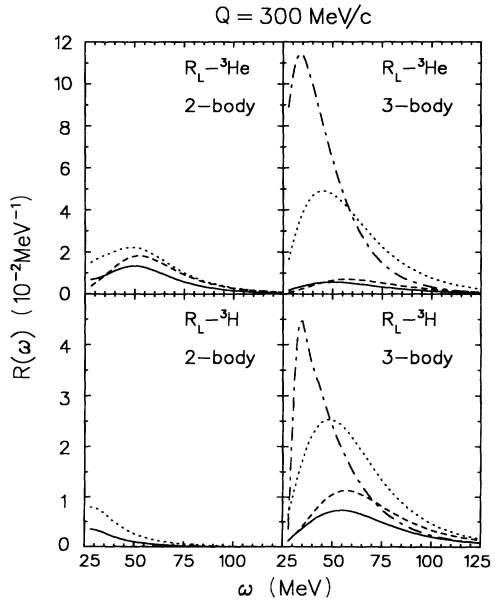

FIG. 12. Two-body and three-body breakup contributions to the longitudinal response of ^{3}He and ^{3}H separately at $Q=300$ MeV/c. The various curves are the same as in Fig. 11.

B. Exclusive kinematics

Instead of the integrated response observables we may consider the nuclear structure functions from Eq. (4), corresponding to the $(e,e'p)NN$ reaction, in order to get more insight in the importance of FSI. In terms of center-of-mass kinematic variables it is a function of the relative kinetic energy $\varepsilon=\sqrt{s_{\text{c.m.}}-q_f^2}$ of the outgoing pair and the relative angle $\theta_f=\hat{\mathbf{q}}_f\cdot\hat{\mathbf{Q}}$. The presented results are obtained with relativistic kinematics. Figure 13 displays a contour plot of the ratio W_C/W_C^{PWIA} for ^{3}He

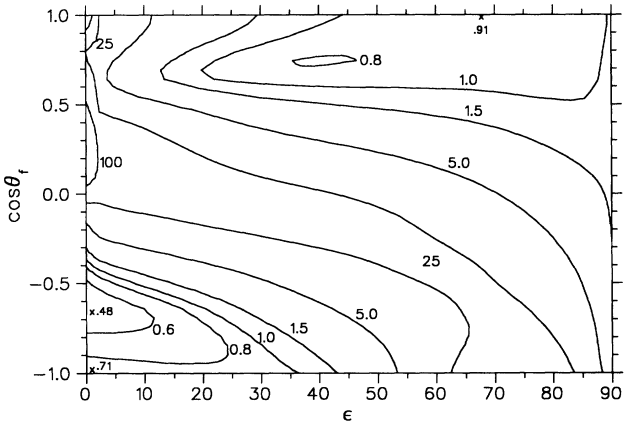

FIG. 13. Contour plot of the ratio W_C/W_C^{PWIA} of the longitudinal nuclear structure functions corresponding to the coincidence ^{3}He$(e,e'p)$ reaction. The momentum transfer Q is 500 MeV/c, while the center-of-mass kinetic energy $s_{\text{c.m.}}$ is 90 MeV. The relative kinetic energy ε of the unobserved pair is in units MeV.

in this two-dimensional space. The momentum transfer is 500 MeV/c and for the energy we have taken $\bar{s}_{\text{c.m.}} = 90$ MeV, which is close to the quasielastic point. The main contribution in the region at $\epsilon = 0$ and $\cos\theta_f = -1$ is due to the PWIA-type diagrams, in which the measured proton is the knocked-out nucleon. The second region, where a PWIA contribution is important, is located at $\epsilon = \frac{3}{4}\bar{s}_{\text{c.m.}}$ and $\cos\theta_f = 1$. Near this kinematic point we are in a typical quasifree situation, where one of the unobserved nucleons is knocked out directly. In both regions, inclusion of the additional disconnected amplitude from Fig. 2(b) together with the connected amplitudes from Figs. 2(c) and 2(d) leads to a reduction of the PWIA contributions [(Fig. 2(a)], which show up as strong and narrow peaks in the three-body breakup nuclear structure function W_C. Off the quasifree kinematic regions, the process of direct nucleon knockout is suppressed and W_C is mainly determined by the remaining diagrams of Fig. 2.

In Fig. 14 the absolute values of the nuclear structure functions are shown as a function of ϵ at some values of θ_f. The pronounced PWIA contributions are clearly present in the plots for (anti)parallel kinematics. In the same subplots the Born calculation has a secondary maximum, which corresponds to the direct knockout of a correlated pair. But these maxima are not pronounced; in fact, they are not significantly larger than the maxima in the off parallel plots. From this it may be understood why the Born response, which results from an integration over ϵ and θ_f, is so enhanced compared to the PWIA response. Furthermore, it may be concluded that in general none of the various truncations of the diagrammatic series of Fig. 2 are reliable approximations of the full result. Only in kinematic regions near the quasielastic point does PWIA lead to a satisfactory description.

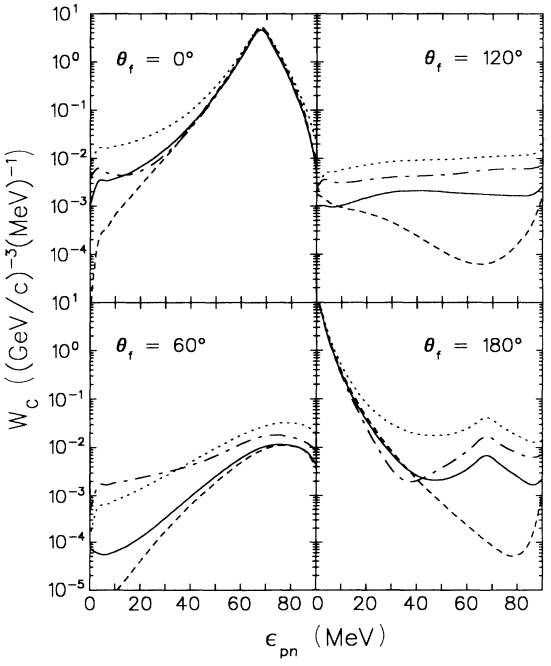

FIG. 14. The longitudinal nuclear structure functions W_C corresponding to the coincidence ^{3}He$(e,e'p)pn$ reaction as a function of the kinetic energy ϵ of the unobserved pair at a number of proton angles θ_f. The various curves are the same as in Fig. 11.

In order to study final-state effects in even more detail we have also considered a number of completely exclusive kinematic setups for the $(e,e'2N)$ breakup reactions. The choices of the kinematic configurations were inspired by previous studies of breakup into three free nucleons in *nd* scattering [15]. In all cases we have restricted ourselves to in-plane reactions. In particular, we have considered a momentum transfer $Q = 300$ MeV/c and a center-of-mass energy $\bar{s}_{\text{c.m.}} = 30$ MeV. In the first example the kinematics is chosen such that in the c.m. frame of the three-nucleon final state the nucleons come out with the same energy and with a relative angle of 120°. It is closely connected to the symmetric, constant-relative-energy (SCRE) loci studied in some detail in *nd* breakup reactions. With the above constraints the only free kinematic parameter is the overall orientation of the triangle of final momenta in the reaction plane with respect to the momentum transfer.

In Fig. 15 the results are displayed as a function of this orientation. We see that the full calculation seems to be somewhat out of phase with the PWIA result. The reason the latter is so small is related to the fact that this kinematics is not even close to a quasielastic point. Once more this is an example where the Born and rescattering approximations lead to results quite different from the full result, in this case one order of magnitude too large.

As a last example Fig. 16 shows the results for the ^{3}H $(e,e'np)p$ cross section at the same values for Q and $\bar{s}_{\text{c.m.}}$ as in Fig. 15. The different kinematics, however, corresponds to the situation of quasifree scattering in *nd* scattering, if one would assume that the triton consisted

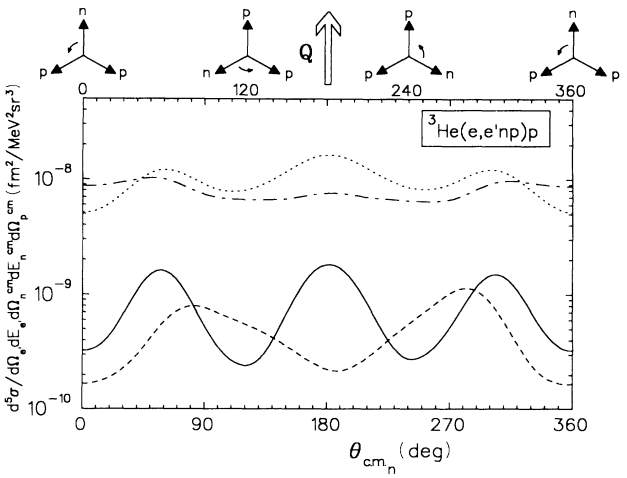

FIG. 15. The exclusive ^{3}He$(e,e'np)p$ breakup reaction at $Q = 300$ MeV/c and $\bar{s}_{\text{c.m.}} = 30$ MeV as a function of the orientation of the triangle in the reaction plane. The kinematic situation is such that in the c.m. system of the three outgoing nucleons, the three nucleons come out under 120° and have equal energy. The various curves are the same as in Fig. 11. The electron parameters are $E_{\text{el}} = 500$ MeV and $\theta_{\text{el}} = 36°$.

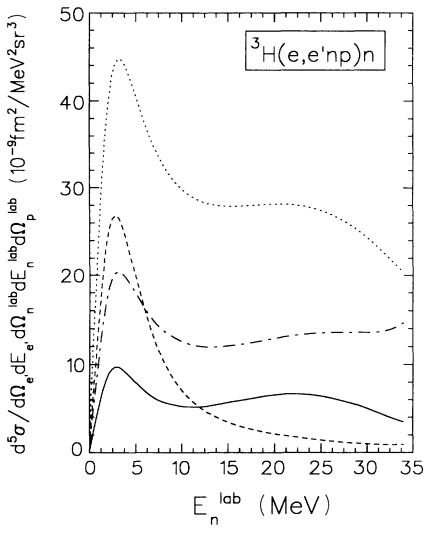

FIG. 16. The exclusive ^{3}He$(e,e'np)p$ breakup reaction at $Q=300$ MeV/c and $\tilde{s}_{c.m.}=30$ MeV as a function of the laboratory energy of the observed neutron. The various curves are the same as in Fig. 11. The electron parameters are the same as in Fig. 15.

of a deuteron and a nucleon after the photon is absorbed by the nucleon with the deuteron at rest. The observed proton and neutron come out in the target rest frame with different energies, but symmetrically under 30° with respect to Q. The PWIA result exhibits a peak at an energy of the detected neutron which corresponds to the situation where the relative momentum between the nonsymmetrically moving neutron and the observed neutron almost vanishes. In the full calculation a second maximum is present at higher neutron energy. This structure already shows up when the photon-correlated-pair diagram is included. This kinematic point corresponds to an almost quasifree situation, i.e., in the target rest frame the nonsymmetrically moving neutron is parallel to the photon momentum and nearly at rest, while the symmetrically emitted nucleons have the same kinetic energy.

V. SUMMARY

In conclusion, we have presented the analysis of the electron-induced three-body breakup process of the trinucleon system. Within the nonrelativistic approach the dynamical equations for both the ground state and the final state have been solved exactly for s-wave N-N interactions. In order to compare the calculated results with the experimental data it is found necessary to introduce relativistic kinematics. A prescription is formulated to link this aspect of relativity to the nonrelativistic nuclear dynamics. It is furthermore verified that UPA can indeed be considered as a valuable tool in the actual calculations of the three-body breakup process.

Results for the trinucleon response functions are shown at three values of the momentum transfer, i.e., $Q=300$, 400, and 500 MeV/c. In general, a full calculation gives a reasonable description of the experimental data for the longitudinal response. Final-state effects are found to play a significant role in renormalizing the PWIA description for the longitudinal response, while the effect of FSI is less pronounced in the calculation of the transverse response. For each of the momentum transfer values the transverse response data are substantially underestimated by a full calculation, which might be ascribed to the absence of meson-exchange currents in this analysis.

In addition, we have studied semi-exclusive $(e,e'N)NN$ and exclusive $(e,e'NN)N$ reactions for some specific kinematic situations. In order to describe these reactions properly one must take into account contributions from the complete multiple scattering series, since the analysis of the various truncations of this series in general leads to quite different results.

ACKNOWLEDGMENTS

Part of the research has been carried out at the Tri-University Meson Facility (TRIUMF) in Vancouver, B.C., Canada, where one of us (E.v.M) has been working in the Theory Group. This work was partially financed by the Stichting voor Fundamenteel Onderzoek der Materie (FOM), which is sponsored by NWO. Part of the numerical computations have been performed on a CYBER 205. This was made possible by the Stichting SURF, The Netherlands.

APPENDIX A: NOTATION

In a nonrelativistic theory, three particles, each with spin $\frac{1}{2}$ and isospin $\frac{1}{2}$, can be represented by normalized states

$$|\mathbf{k}_1\mathbf{k}_2\mathbf{k}_3 s_1^z s_2^z s_3^z t_1^z t_2^z t_3^z\rangle \ , \tag{A1}$$

where $\mathbf{k}_i$ denotes the momentum of particle i and s_i^z, t_i^z label the spin and isospin component of particle i. The kinetic energy of this state is

$$E_0=\mathbf{k}_1^2/2M_1+\mathbf{k}_2^2/2M_2+\mathbf{k}_3^2/2M_3 \ . \tag{A2}$$

Hereafter, we only consider nucleons with equal mass M_N. To split off the center-of-mass motion we introduce the relative momenta

$$\begin{aligned}\mathbf{K}&=\mathbf{k}_1+\mathbf{k}_2+\mathbf{k}_3 \ ,\\ \mathbf{k}_{p_i}&=\tfrac{1}{2}(\mathbf{k}_j-\mathbf{k}_k) \ ,\\ \mathbf{k}_{q_i}&=\tfrac{1}{3}(\mathbf{k}_j+\mathbf{k}_k-2\mathbf{k}_i) \ ,\end{aligned} \tag{A3}$$

where (ijk) is a cyclic permutation of (123). It is convenient to eliminate the masses from the energy of the relative motion by introducing scaled relative momenta

$$\mathbf{p}_i=\left[\frac{1}{M_N}\right]^{1/2}\mathbf{k}_{p_i} \quad \text{and} \quad \mathbf{q}_i=\frac{1}{2}\left[\frac{3}{M_N}\right]^{1/2}\mathbf{k}_{q_i} \ . \tag{A4}$$

In this way the kinetic energy becomes

$$E_0=\frac{1}{6M_N}\mathbf{K}^2+\mathbf{p}^2+\mathbf{q}^2 \ , \tag{A5}$$

where indices on p and q would be redundant. Throughout the entire paper, we use the so-called Jacobi

coordinates of Eq. (A4). If we consider only the momenta, the relevant part of Eq. (A1) becomes

$$|\mathbf{p}_i\mathbf{q}_i\rangle_i \ . \tag{A6}$$

Since there are three particles, Eq. (A6) represents three equivalent states, and as mentioned before $p_i^2+q_i^2$ does not depend on the label. It is essential to note that the indices i in Eq. (A6) have different meanings. The index on the ket $|\ \rangle$ refers to the coupling scheme adopted in Eq. (A3), i.e., first $j+k\rightarrow(jk)$ and then $(jk)+i\rightarrow(jk)i$, whereas the index on the momentum just expresses that particle i has a momentum $\mathbf{k}_i$.

Since we are dealing with identical particles, the three-nucleon wave functions must be antisymmetric with respect to a permutation operation

$$P_i^{\text{total}}=P_i^{\text{space}}P_i^{\text{spin}}P_i^{\text{isospin}} \ .$$

The operators P_i $(i=1,2,3)$, which interchange the labels of particle j and k, form the odd elements of the permutation group S_3. The even elements of S_3 are the identity e, and the operators P_{jki} and P_{kij}, which perform a cyclic shift of the arrangement (ijk). From the elements of S_3 we can construct the antisymmetrizer

$$A_3=A_{2_i}P_s \ , \tag{A7}$$

with

$$P_s=\frac{1}{\sqrt{3}}(e+P_{231}+P_{312}) \tag{A8}$$

and

$$A_{2_i}=\frac{1}{\sqrt{2}}(1-P_i) \ . \tag{A9}$$

P_s antisymmetrizes a three-nucleon state that is antisymmetric in at least one pair. Such a state is constructed by A_{2_i} operating on an arbitrary three-nucleon state. The operator A_3 does not depend on the index i.

At this point, it is straightforward to introduce a new set of basis states which are antisymmetric with respect to at least one pair:

$$\begin{aligned}|\mathbf{pq}\beta\rangle_i^A&=A_{2_i}|\mathbf{pq}\beta\rangle_i \ ,\\ |\alpha\mathbf{q}\beta\rangle_i^A&=A_{2_i}|\alpha\mathbf{q}\beta\rangle_i \ .\end{aligned} \tag{A10}$$

Here α labels a two-nucleon bound state and β represents all remaining spin-isospin quantum numbers Since the basis states $|\mathbf{pq}\beta\rangle_i$ and $|\alpha\mathbf{q}\beta\rangle_i$ are normalized to "one," the partially antisymmetrized states from Eq. (A10) have the normalization

$$\begin{aligned}{}_i^A\langle\mathbf{pq}\beta|\mathbf{pq}\beta'\rangle_i^A&=\delta_{\beta\beta'}\delta(\mathbf{q}-\mathbf{q}')\\ &\quad\times[\delta(\mathbf{p}-\mathbf{p}')-(-1)^{\beta_p}\delta(\mathbf{p}+\mathbf{p}')] \ ,\end{aligned} \tag{A11}$$

$${}_i^A\langle\alpha\mathbf{q}\beta|\alpha'\mathbf{q}'\beta'\rangle_i^A=2\delta_{\beta\beta'}\delta(\mathbf{q}-\mathbf{q}')\delta_{\alpha\alpha'} \ .$$

The effective closure relations are

$$\begin{aligned}\mathbf{I}&=\sum_\beta\int d\mathbf{p}\,d\mathbf{q}|\mathbf{pq}\beta\rangle_{i\ i}\langle\mathbf{pq}\beta| \ ,\\ \mathbf{I}&=\tfrac{1}{2}\sum_\beta\int d\mathbf{p}\,d\mathbf{q}|\mathbf{pq}\beta\rangle_i^{A\ A}\langle\mathbf{pq}\beta| \ .\end{aligned} \tag{A12}$$

From Eq. (A3) it is obvious that the momenta $(\mathbf{p}_i,\mathbf{q}_i)$ form three dependent sets for the values $i=1,2,3$. The relations are linear and we can construct a 2×2 matrix α_{ji} such that

$$\begin{bmatrix}\mathbf{p}_j\\ \mathbf{q}_j\end{bmatrix}=\alpha_{ji}\begin{bmatrix}\mathbf{p}_i\\ \mathbf{q}_i\end{bmatrix} \ , \tag{A13}$$

with (ijk) cyclic. In case of the above choice of relative momenta we have

$$\alpha_{ji}=\begin{bmatrix}-\frac{1}{2} & +\frac{1}{2}\sqrt{3}\\ -\frac{1}{2}\sqrt{3} & -\frac{1}{2}\end{bmatrix} \ , \tag{A14}$$

with properties $\det\alpha=1,(\alpha_{ji})^3=\mathbf{I},(\alpha_{ji})^{-1}=\alpha_{ij}$. The sets $(\mathbf{p}_j,\mathbf{q}_j)$ and $(\mathbf{p}_i,\mathbf{q}_i)$ are called mutually associated momenta.

Furthermore, we have to consider the nucleonic spin and isospin degrees of freedom. At this level these quantum numbers are entirely independent, and complete quantum states are found by taking the direct product of spin and isospin states. Although the set of spin states $|s_1^zs_2^zs_3^z\rangle$ in Eq. (A1) form a complete set, it is convenient to introduce orthonormal states

$$|(s_js_k)s_ps_q;SS^z\rangle_i \ , \tag{A15}$$

where s_q is the spin of the spectator particle i and (ijk) again forms a cyclic order of (123). S and S^z denote the total spin and spin component of the three-nucleon state. The spins combine to $S=\frac{1}{2}$ (doublet) or $S=\frac{3}{2}$ (quartet). The spin number s_p arises from coupling the nucleon spins s_j and s_k. It either takes the value $s_p=0$ (singlet) or $s_p=1$ (triplet). The combination $s_p=0,S=\frac{3}{2}$ is excluded. Equation (A15) represents three spin states, if we ignore the magnetic spin component S^z. In analysis with only S-wave N-N interactions, this is a valid assumption and accordingly we introduce an abbreviated form of Eq. (A15):

$$|\chi_m^r\rangle_i \ , \tag{A16}$$

where r takes the values doublet or quartet and m takes the values singlet or triplet. Since the nucleonic spin and isospin are both $\frac{1}{2}$, treatment of these quantum numbers is entirely equivalent, and we introduce isospin basis states

$$|\eta_m^r\rangle_i \ , \tag{A17}$$

where the meaning of the labels is similar to Eq. (A16). To represent the spin-isospin states, we will often use the shorthand notation

$$|\beta\rangle_i=|(s_js_k)s_ps_qSS^z;(t_jt_k)t_pt_qTT^z\rangle_i \ . \tag{A18}$$

The three-body analysis requires knowledge of the spin-isospin recoupling matrix elements ${}_j\langle\beta'|\beta\rangle_i$. In the recoupling, the total spin (isospin) is conserved. For the

spin-doublet state we obtain with the aid of Edmonds' general recoupling coefficient [16]

$$ {}_j\langle \chi^d_{m'}|\chi^d_m\rangle_i = \begin{bmatrix} -\frac{1}{2} & +\frac{1}{2}\sqrt{3} \\ -\frac{1}{2}\sqrt{3} & -\frac{1}{2} \end{bmatrix} , \tag{A19} $$

where $m,m'=(s,t)$, and (ijk) is a fixed cyclic permutation of (123). To rule out any confusion, we explicitly state that in the chosen convention

$$ {}_2\langle \chi^d_t|\chi^d_s\rangle_1 = -\tfrac{1}{2}\sqrt{3} . \tag{A20} $$

The complete spin-isospin recoupling matrix restricted to pure doublet states therefore is

$$ B_{ji} = {}_j\langle \chi^d|\chi^d\rangle_i \otimes {}_j\langle \eta^d|\eta^d\rangle_i = \begin{bmatrix} \frac{1}{4} & -\frac{3}{4} & \frac{1}{4}\sqrt{3} & -\frac{1}{4}\sqrt{3} \\ -\frac{3}{4} & \frac{1}{4} & \frac{1}{4}\sqrt{3} & -\frac{1}{4}\sqrt{3} \\ -\frac{1}{4}\sqrt{3} & -\frac{1}{4}\sqrt{3} & \frac{1}{4} & \frac{3}{4} \\ \frac{1}{4}\sqrt{3} & \frac{1}{4}\sqrt{3} & \frac{3}{4} & \frac{1}{4} \end{bmatrix} , \tag{A21} $$

where both the row and the column sequence of spin-isospin states is given by $\chi_t\eta_s$, $\chi_s\eta_t$, $\chi_s\eta_s$, $\chi_t\eta_t$. The matrix B_{ji} has the same properties as α_{ji}. The spin-quartet recoupling is considerably simpler, since it involves only one channel

$$ {}_j\langle \chi^q_t|\chi^q_t\rangle_i = 1 . \tag{A22} $$

In the entire analysis we will regard particle 1 as the spectator particle, unless mentioned else.

APPENDIX B: RELATIVISTIC PHASE SPACE FACTOR

In order to derive the relativistic phase space factor related to the three-body breakup contribution to the response functions we start from an integral in the laboratory frame. Hereafter the spin-isospin dependence is omitted, as the phase space factor has a purely kinematic origin. This factor arises in the integration of the squared amplitude over all possible values for the particle momenta in the laboratory frame:

$$ R = \int \prod_{i=1}^{3} d\mathbf{k}_i \delta^{(3)}\left[\sum_{i=1}^{3}\mathbf{k}_i - \mathbf{Q}\right] \times \delta\left[\sum_{i=1}^{3}\varepsilon_i - \omega - M_t\right] |M|^2 , \tag{B1} $$

where $\varepsilon_i = \sqrt{k_i^2 + M_N^2}$ is the relativistic energy of particle i. Of course, the quantity R is related to the response function, while M corresponds to the three-body breakup amplitude. The δ functions restrict the phase space to the regions where conservation of momentum and energy is satisfied. In practice we cast Eq. (B1) into an integral over the Jacobi coordinates $\mathbf{p}_f$ and $\mathbf{q}_f$. First we introduce the corresponding center-of-mass momenta by means of a Lorentz transformation,

$$ \mathbf{k}_i^{(\mathrm{c.m.})} = \mathbf{k}_i + \boldsymbol{\beta}\gamma\left[\frac{\gamma}{\gamma+1}\boldsymbol{\beta}\cdot\mathbf{k}_i - \varepsilon_i\right] , \qquad \varepsilon_i^{(\mathrm{c.m.})} = \gamma(\varepsilon_i - \boldsymbol{\beta}\cdot\mathbf{k}_i) . \tag{B2} $$

Invariance of four-momentum transfer links the energy transfer ω to the total kinetic energy $s_{\mathrm{c.m.}}$ in the c.m. frame,

$$ (s_{\mathrm{c.m.}} + 3M_N)^2 = (\omega + M_T)^2 - \mathbf{Q}^2 . \tag{B3} $$

Consequently the transformation velocity β and the related quantity $\gamma = 1/\sqrt{1-\beta^2}$ are given by

$$ \boldsymbol{\beta} = \frac{\mathbf{Q}}{\omega + M_T} \quad \text{and} \quad \gamma = \frac{\omega + M_T}{s_{\mathrm{c.m.}} + 3M_N} . \tag{B4} $$

The center-of-mass momenta are chosen as the new set of integration variables in Eq. (B1), which gives rise to a Jacobi factor

$$ J_1 = \left|\gamma^3 \prod_{i=1}^{3}\left[1 + \frac{\boldsymbol{\beta}\cdot k_i^{(\mathrm{c.m.})}}{\varepsilon_i^{(\mathrm{c.m.})}}\right]\right| . \tag{B5} $$

In the next step we replace the center-of-mass momenta by the relative momenta $\mathbf{k}_p$ and $\mathbf{k}_q$ and by the total momentum $\mathbf{K}$ from Eq. (A3). After some rearrangements we find that the quantity R from Eq. (B1) can be written as

$$ R = \int d\mathbf{k}_q d\mathbf{k}_p d\mathbf{K}\, J_1 |M|^2 \delta^{(2)}(\mathbf{K}^{\perp})\delta^{(1)}(\gamma K^z + \gamma\beta E^{(\mathrm{c.m.})} - Q)\delta^{(1)}(\gamma E^{(\mathrm{c.m.})} + \gamma\beta K^z - \omega - M_T) , \tag{B6} $$

where $E^{(\mathrm{c.m.})} = \sum_{i=1}^{3}\varepsilon_i^{(\mathrm{c.m.})}$. While the integration over the transverse components $\mathbf{K}^{\perp}$ to the momentum transfer can be done trivially, the integral over the longitudinal component K^z requires some more attention. First it may be rewritten as

$$ \int dK^z \frac{\delta^{(1)}(K^z - f_0)}{|[\partial f(K^z)/\partial K^z]_{K^z=f_0}|} \frac{\delta^{(1)}(K^z - g_0)}{|[\partial g(K^z)/\partial K^z]_{K^z=g_0}|} , \tag{B7} $$

with

$$f(K^z,E^{(\mathrm{c.m.})})=\gamma(K^z+\beta E^{(\mathrm{c.m.})})-Q\ ,$$
$$g(K^z,E^{(\mathrm{c.m.})})=\gamma(E^{(\mathrm{c.m.})}+\beta K^z)-\omega-M_T\ ,$$

and

$$f_0=Q/\gamma-\beta E^{(\mathrm{c.m.})}\ ,$$
$$g_0=(\omega+M_T)/\gamma-E^{(\mathrm{c.m.})}/\beta\ .$$

Elimination of the energy $E^{(\mathrm{c.m.})}$ shows that the solution $K^z=0$ is the only common root of the δ-function arguments. Therefore the integral in Eq. (B7) over K^z yields

$$J_2=\gamma^2\beta\delta^{(1)}(H_0(\mathbf{k}_p,\mathbf{k}_q)-s_{\mathrm{c.m.}})|\gamma[1+\beta(\partial H_0/\partial K^z)_{K^z=0}]\gamma[(\partial H_0/\partial K^z)_{K^z=0}+\beta]|^{-1}\ , \tag{B8}$$

where the kinetic energy H_0 is given by

$$H_0(\mathbf{k}_p,\mathbf{k}_q)=\sum_{i=1}^{3}\varepsilon_i^{(\mathrm{c.m.})}(\mathbf{k}_p,\mathbf{k}_q)-3M_N=\sqrt{k_q^2+M_N^2}+\sqrt{(\mathbf{k}_p+\tfrac{1}{2}\mathbf{k}_q)^2+M_N^2}+\sqrt{(-\mathbf{k}_p+\tfrac{1}{2}\mathbf{k}_q)^2+M_N^2}\ . \tag{B9}$$

The derivative factor becomes

$$(\partial H_0/\partial K^z)_{K^z=0}=\frac{-\frac{1}{3}\mathbf{k}_q\cdot\hat{\mathbf{z}}}{\varepsilon_1^{(\mathrm{c.m.})}}+\frac{(\frac{1}{3}\mathbf{k}_p+\frac{1}{6}\mathbf{k}_q)\cdot\hat{\mathbf{z}}}{\varepsilon_2^{(\mathrm{c.m.})}}+\frac{(-\frac{1}{3}\mathbf{k}_p+\frac{1}{6}\mathbf{k}_q)\cdot\hat{\mathbf{z}}}{\varepsilon_3^{(\mathrm{c.m.})}}\ . \tag{B10}$$

In terms of the Jacobi coordinates $\mathbf{p}_f=\mathbf{k}_p/\sqrt{M_N}$ and $\mathbf{q}_f=\frac{1}{2}\mathbf{k}_q\sqrt{3/M_N}$ from Eq. (A4) the result for Eq. (B1) is

$$R=(2M_N/\sqrt{3})^3\int d\mathbf{p}_f d\mathbf{q}_f J_1 J_2|M(\mathbf{p}_f,\mathbf{q}_f;\mathbf{Q},s_{\mathrm{c.m.}})|^2\delta(H_0(\mathbf{p}_f,\mathbf{q}_f)-s_{\mathrm{c.m.}})\ . \tag{B11}$$

The energy conserving δ function is removed by integrating over p_f. This gives rise to a phase space factor

$$k_f=p_f^2\left|\frac{\partial H_0(\mathbf{p}_f,\mathbf{q}_f)}{\partial p_f}\right|^{-1}_{H_0=s_{\mathrm{c.m.}}}\ . \tag{B12}$$

In the relativistic case the solution for p_f^2 is given by

$$p_f^2(q_f,x_{p_fq_f})=(s_{\mathrm{c.m.}}+3M_N-E_{q_f})^2\left[\frac{(s_{\mathrm{c.m.}}+3M_N-E_{q_f})^2-E_{q_f}-3M_N^2}{4M_N(s_{\mathrm{c.m.}}+3M_N-E_{q_f})^2-(4M_Nq_fx_{p_fq_f})^2/3}\right]\ , \tag{B13}$$

where $E_{q_f}=\sqrt{\frac{4}{3}M_Nq_f^2+M_N^2}$ and $x_{p_fq_f}=\hat{\mathbf{p}}_f\cdot\hat{\mathbf{q}}_f$. The corresponding phase space factor takes the form

$$k_f=p_f^2\left|\frac{p+q_fx_{p_fq_f}/\sqrt{3}}{\sqrt{1+(\mathbf{p}_f+\mathbf{q}_f/\sqrt{3})^2/M_N}}+\frac{p-q_fx_{p_fq_f}/\sqrt{3}}{\sqrt{1+(\mathbf{p}_f-\mathbf{q}_f/\sqrt{3})^2/M_N}}\right|^{-1}\ . \tag{B14}$$

The accessible phase space is bounded by the rectangle $[(0,p_{\max}),(0,q_{\max})]$, with

$$p_{\max}^2=s_{\mathrm{c.m.}}(1+\tfrac{1}{4}s_M)\ ,$$
$$q_{\max}^2=s_{\mathrm{c.m.}}\frac{(1+\frac{11}{12}s_M+\frac{1}{4}s_M^2+\frac{1}{48}s_M^3)}{(1+\frac{2}{3}s_M+\frac{1}{9}s_M^2)}\ , \tag{B15}$$

where $s_M=s_{\mathrm{c.m.}}/M_N$.

In the nonrelativistic limit the above relations simplify considerably. We have in this case $J_1=J_2=1$, so that Eq. (B11) becomes

$$R=(2M_N/\sqrt{3})^3\int d\mathbf{p}_f d\mathbf{q}_f|M(\mathbf{p}_f,\mathbf{q}_f;\mathbf{Q},s_{\mathrm{c.m.}})|^2\times\delta(p_f^2+q_f^2-s_{\mathrm{c.m.}})\ . \tag{B16}$$

Moreover, Eqs. (B12)–(B15) are replaced by the much simpler results

$$p_f^2=s_{\mathrm{c.m.}}-q_f^2\ , \tag{B17}$$
$$k_f=\tfrac{1}{2}p_f\ , \tag{B18}$$
$$p_{\max}^2=s_{\mathrm{c.m.}}\ , \tag{B19}$$
$$q_{\max}^2=s_{\mathrm{c.m.}}\ . \tag{B20}$$

In summary, the quantity R from Eq. (B1) can be rewritten in terms of an integral over the Jacobi coordinates according to

$$R=(2M_N/\sqrt{3})^3\int d\mathbf{q}_f d\Omega_{p_f}J_1J_2k_f|M(\mathbf{p}_f,\mathbf{q}_f;\mathbf{Q},s_{\mathrm{c.m.}})|^2\ , \tag{B21}$$

where we have used relativistic kinematics to describe the motion of the three outgoing particles. The quantities J_1, J_2, and k_f are expressed in Eqs. (B5), (B8), and (B14). Nonrelativistically, we find a similar expression with $J_1=J_2=1$ and k_f according to Eq. (B18). The limits of integration for the q_f variable also slightly change in turning from relativistic to nonrelativistic kinematics.

APPENDIX C: TRIPLE COLLISION TERM

In $3N\rightarrow Nd$ scattering the momentum of the spectator particle is fixed by energy conservation to $q_f^2=s_{\text{c.m.}}-E_d>s_{\text{c.m.}}$. The rescattering term $B^{(1)}$ contains the deuteron wave function which is regular in the variable p. Therefore the function $B^{(1)}_{3N\rightarrow Nd}$ is smooth and can serve as the driving term for the $3N\rightarrow Nd$ scattering series. The $3N\rightarrow 3N$ double collision term takes a similar form. It is proportioanl to the free three-particle propagator, from which we may deduce its analytic structure. In UPA we would have the form

$$B^{(1)}_{3N\rightarrow 3N}\propto\frac{N_d}{p^2+q_f^2-s_{\text{c.m.}}-i\varepsilon}g(p)\ . \tag{C1}$$

Since the outgoing pair is in a continuum state with $p_f^2>0$ and consequently the spectator momentum $q_f^2=s_{\text{c.m.}}-p_f^2<s_{\text{c.m.}}$, we see that the propagator $(p^2+q_f^2-s_{\text{c.m.}})^{-1}$ can become singular. The integration over the variable p gives rise to logarithmic singularities in the q dependence of the double collision term. Although their position as a function of the final spectator momentum q_f is precisely known, due to the logarithmic structure it cannot simply be used as the driving term to generate the $3N\rightarrow 3N$ multiple scattering series. However, the once more iterated term, i.e., triple collision term $B^{(2)}_{3N\rightarrow 3N}$, is sufficiently smooth to be used as the driving term. Hence, once the triple collision term is obtained with sufficient accuracy we may simply use the standard iteration scheme as for the Nd case to calculate the multiple scattering series. From this the solutions to the continuum Faddeev equations are obtained using the Padé approximants of the series.

We now describe in detail how the triple collision term is constructed from the double collision term. Employing the separable s-wave UPA to describe the N-N interaction the $3N\rightarrow 3N$ can be expressed as

$$\begin{aligned}B^{(1)}(\mathbf{p}_1\mathbf{q}_1\beta_1|\mathbf{p}_f\mathbf{q}_f\beta_f)=&\frac{1}{p_1^2+q_1^2-s_{\text{c.m.}}-i\varepsilon}\\&\times g(p_1;\beta_1)\tau(s_{\text{c.m.}}-q_1^2;\beta_1)\\&\times\Psi^{(1)}(\mathbf{q}_1\beta_1|\mathbf{q}_f\beta_f)\\&\times\tau(s_{\text{c.m.}}-q_f^2;\beta_f)g(p_f;\beta_f)\ .\end{aligned}\tag{C2}$$

Here $\mathbf{p}_f,\mathbf{q}_f$ are the Jacobi coordinates of the final state, while $\mathbf{p}_1,\mathbf{q}_1$ form a set of off-shell momenta. The complicated part of $B^{(1)}$ of course is the spectator wave function $\Psi^{(1)}$. At this point we observe that $\Psi^{(1)}$ is nothing else than the half-on-shell part of the kernel K which governs the iterations of the scattering series. In fact, we can just copy K from the $3N\rightarrow Nd$ scattering analysis. More specifically, we have

$$\Psi^{(1)}(\mathbf{q}_1\beta_1|\mathbf{q}_f\beta_f)=2K(\mathbf{q}_1\beta_1|\mathbf{q}_f\beta_f)\ , \tag{C3}$$

where the factor 2 accounts for the relative weight of the rescattering diagrams compared to the disconnected diagrams. The kernel K can be partial wave expanded according to

$$K(\mathbf{q}_1\beta_1|\mathbf{q}_3'\beta')=\sum_l(2l+1)P_l(x_{13'})K_l(q_1;\beta_1|q_3';\beta')\ , \tag{C4}$$

with $x_{13'}=\hat{\mathbf{q}}_1\cdot\hat{\mathbf{q}}_3'$. The corresponding partial wave coefficients can be expressed like

$$K_l(q_1;\beta|q_3';\beta')=\frac{4}{3\sqrt{3}}\int dx'_{13}P_l(x'_{13})\frac{g((2/\sqrt{3})|\mathbf{q}_3'+\frac{1}{2}\mathbf{q}_1|;\beta)_1\langle\beta|\beta'\rangle_3 g((2/\sqrt{3})|\mathbf{q}_1+\frac{1}{2}\mathbf{q}_3'|;\beta')}{\frac{4}{3}(q_1^2+q_3'^2+q_1q_3'x'_{13})-z}\ . \tag{C5}$$

In the numerical evaluation of K_l standard subtraction techniques are used to remove the propagator singularities in the integrand. To anticipate the construction of the triple collision term we restate the expression for K_l as

$$\tfrac{4}{3}q_iq_fK_l(q_i\beta_i|q_f\beta_f)=R_l(q_i\beta_i|q_f\beta_f)+W_l(q_i\beta_i|q_f\beta_f)+iI_l(q_i\beta_i|q_f\beta_f)\ , \tag{C6}$$

where the real-valued functions R, W, and I are given by

$$R_l(q\beta|q'\beta')=\tfrac{1}{2}P\int_{-1}^{+1}dx\ P_l(x)\frac{f(x(q,q');\beta\beta')-f(x_s(q,q');\beta\beta')}{x-x_s}\ , \tag{C7}$$

$$W_l(q\beta|q'\beta')=-Q_l^P(x_s)f(x_s(q,q');\beta\beta')\ , \tag{C8}$$

$$I_l(q\beta|q'\beta')=\tfrac{1}{2}\pi\int_{-1}^{+1}dy\ P_l(y)f(y(q,q');\beta\beta')\delta(y-x_s)\ , \tag{C9}$$

with

$$x_s=\frac{\frac{3}{4}s_{\text{c.m.}}-q^2-q'^2}{qq'} \tag{C10}$$

and

$$f(x(q,q');\beta\beta')=g\left[\frac{2}{\sqrt{3}}|\mathbf{q}'+\tfrac{1}{2}\mathbf{q}|;\beta\right]{}_1\langle\beta|\beta'\rangle_3 g\left[\frac{2}{\sqrt{3}}|\mathbf{q}+\tfrac{1}{2}\mathbf{q}'|;\beta'\right] . \tag{C11}$$

The function I_l is obviously restricted to the three-nucleon region enclosed by the curves $x_s(q,q')=\pm 1$. In the expression for W_l we have introduced the principal value of the Legendre function of the second kind Q_l defined as

$$Q_l^P(y)=\tfrac{1}{2}P\int_{-1}^{+1}dx\frac{P_l(x)}{y-x} . \tag{C12}$$

It compensates the subtraction term in R_l, which is added in order to obtain a regular principal value integral. At threshold the Q_l^P functions contain logarithmic singularities. The threshold curve $x_s(q,q')=\pm 1$ is displayed in Fig. 17. The corresponding threshold function $q'(q)$ is given by

$$\left.\begin{aligned} q'&=-\tfrac{1}{2}[q-\sqrt{3(s_{\text{c.m.}}-q^2)}] \quad x_s=+1 , \\ q'&=\tfrac{1}{2}[q+\sqrt{3(s_{\text{c.m.}}-q^2)}] \\ q'&=\tfrac{1}{2}[q-\sqrt{3(s_{\text{c.m.}}-q^2)}] \end{aligned}\right\} \quad x_s=-1 . \tag{C13}$$

The free scattering space is enclosed by the square $(q,q')=([0,\sqrt{s_{\text{c.m.}}}],[0,\sqrt{s_{\text{c.m.}}}])$, the area to which the subtraction is confined. The contribution I_l is limited to the area enclosed by the threshold curves $x_s(q',q)$.

To calculate the triple collision term we introduce the convolution $K_l^{(2)}$ of two double collision terms K_l according to

$$(\tfrac{4}{3})^2 q_i q_f K_l^{(2)}(q_i\beta_i|q_f\beta_f)=\sum_\beta\int dq(\tfrac{4}{3}q_i q)K_l(q_i\beta_i|q\beta)\tau(s_{\text{c.m.}}-q^2;\beta)(\tfrac{4}{3}qq_f)\psi_l^{(1)}(q\beta|q_f\beta_f) . \tag{C14}$$

We rewrite the right-hand side of Eq. (C14) in order to single out the logarithmic contribution

$$2\sum_\beta\int dq\{[R_l(q_i\beta_i|q\beta)+iI_l(q_i\beta_i|q\beta)]\tau(s_{\text{c.m.}}-q^2;\beta)[R_l(q\beta|q_f\beta_f)+iI_l(q\beta|q_f\beta_f)]\} \tag{C15}$$

and

$$\begin{aligned} 2\sum_\beta\int dq\{&[R_l(q_i\beta_i|q\beta)+iI_l(q_i\beta_i|q\beta)]\tau(s_{\text{c.m.}}-q^2;\beta)W_l(q\beta|q_f\beta_f) \\ &+W_l(q_i\beta_i|q\beta)\tau(s_{\text{c.m.}}-q^2;\beta)[R_l(q\beta|q_f\beta_f)+iI_l(q\beta|q_f\beta_f)]+W_l(q_i\beta_i|q\beta)\tau(s_{\text{c.m.}}-q^2;\beta)W_l(q\beta|q_f\beta_f)\} . \end{aligned} \tag{C16}$$

Except for the deuteron pole in the τ function the integrand in the first contribution is a regular function of q. The second contribution, however, contains logarithms of the form

$$\ln[|q-q_\omega(q,q')|] , \tag{C17}$$

where $q_\omega(q,q')$ are the threshold points

$$\left.\begin{aligned} q_{\omega_1}&=\tfrac{1}{2}|q-\sqrt{3(s_{\text{c.m.}}-q^2)}| , \\ q_{\omega_2}&=\tfrac{1}{2}[q+\sqrt{3(s_{\text{c.m.}}-q^2)}] . \end{aligned}\right. \tag{C18}$$

The logarithms are integrable and after the convolution of the kernels the form in expression (C17) has turned into a harmless algebraic-logarithmic dependence

$$[q-q_\omega(q,q')]\ln[|q-q_\omega(q,q')|] . \tag{C19}$$

To determine $K_l^{(2)}$ numerically we have applied the following procedure. Both integrals (C15) and (C16) heavily depend on the position of q_i and q_f. The most complicated situation occurs when q_i and q_f have both continuum values: $q_i^2,q_f^2<s_{\text{c.m.}}$. In that case the continuum sector contains two threshold curves (see Fig. 17): $q=q(q_i)$ and $q=q(q_f)$. Both relations are according to expression (C13). Consequently four branch points $(q_{\omega_{1_i}},q_{\omega_{2_i}},q_{\omega_{1_f}},q_{\omega_{2_f}})$ exist [Eq. (C18)], which are arranged in increasing order q_{b_k} $(k=1,4)$.

For some values of q_i and q_f these branch points coincide. Of course, if $q_i=q_f$ then $q_{\omega_i}=q_{\omega_f}$, but more coincidences of q_i with either q_f, $q_{\omega_{1_f}}$, or $q_{\omega_{2_f}}$ occur:

	$q_i \in [0, \frac{1}{2}\sqrt{s_{\text{c.m.}}}]$	$q_i \in [\frac{1}{2}\sqrt{s_{\text{c.m.}}}, \frac{1}{2}\sqrt{3s_{\text{c.m.}}}]$	$q_i \in [\frac{1}{2}\sqrt{3s_{\text{c.m.}}}, \sqrt{s_{\text{c.m.}}}]$
$q_f \in [0, \frac{1}{2}\sqrt{s_{\text{c.m.}}}]$	$q_i = q_f$	$q_i = q_{\omega_{1_f}}$	$q_i = q_{\omega_{2_f}}$
$q_f \in [\frac{1}{2}\sqrt{s_{\text{c.m.}}}, \frac{1}{2}\sqrt{3s_{\text{c.m.}}}]$	$q_i = q_{\omega_{1_f}}$	$q_i = q_f$	$q_i = q_{\omega_{2_f}}$
$q_f \in [\frac{1}{2}\sqrt{3s_{\text{c.m.}}}, \sqrt{s_{\text{c.m.}}}]$	$q_i = q_{\omega_{1_f}}$	$q_i = q_{\omega_{2_f}}$	$q_i = q_f$

The coincidences are determined by the subinterval to which the values of q_i and q_f are restricted. For example, if $q_i = q_{\omega_{1_f}}$, then either $q_{\omega_{1_i}} = q_{\omega_{2_f}}$ and $q_{\omega_{2_i}} = q_f$ or $q_{\omega_{1_i}} = q_f$ and $q_{\omega_{2_i}} = q_{\omega_{2_f}}$.

With the above analysis on the positions of the various branch points in mind we can arrange for a proper distribution of the integration points q. It is stressed that the way the q points are scattered is decisive in achieving an adequate integration procedure. Let us discuss the situation where all four branch points are different.

To perform the regular integration in Eq. (C15) Gauss-Legendre quadratures are employed for each of the five subranges of the interval $[0, \sqrt{s_{\text{c.m.}}}]$ according to the following scheme:

	0	q_{b_1}	q_{b_2}	q_{b_3}	q_{b_4}	$\sqrt{s_{\text{c.m.}}}$
Gauss-Legendre q mesh	n_g	$n_{\text{reg}}^{(1)}$	$n_{\text{reg}}^{(2)}$	$n_{\text{reg}}^{(3)}$	n_g	
Gauss-Laguerre q mesh	$\frac{1}{2}n_g$ $n_{\omega_R}^{(1)}$	$n_{\omega_L}^{(1)}$ $n_{\omega_R}^{(2)}$	$n_{\omega_L}^{(2)}$ $n_{\omega_R}^{(3)}$	$n_{\omega_L}^{(3)}$ $n_{\omega_R}^{(4)}$	$n_{\omega_L}^{(4)}$ $\frac{1}{2}n_g$	

The number of points in the first and last range is set to $n_g = 4$. In the remaining intervals the number depends on the width of the interval, but is bound on both sides: $8 \le n \le n_{\text{reg}_{\max}}$. The value $n_{\text{reg}_{\max}} = 24$ turns out to be in general a good choice, except when the intervals become narrow. In that case we found that a value for n smaller than $n_{\text{reg}_{\max}}$ led to more stable results.

To perform the logarithmic integrals in Eq. (C16), Gauss-Laguerre quadratures are employed such that integrals of the form $\int_{a<b}^{b} f(q)\ln(b-q)dq$ are accounted for exactly. The five intervals are each divided into two subintervals such as shown in the above scheme. Only the integrations in the first and last interval are done with a Gauss-Legendre quadrature for $n_g/2 = 2$ points. In the remaining eight intervals the entire integral in Eq. (C16) is carried out with Gauss-Laguerre quadratures regardless of the fact that at each branch point the logarithmic singularity is present in only one term of the integrand. The values for $n_{\omega_R^{(i)}}$, $n_{\omega_L^{(i)}}$ are selected with respect to the width of the subinterval, in the restriction that

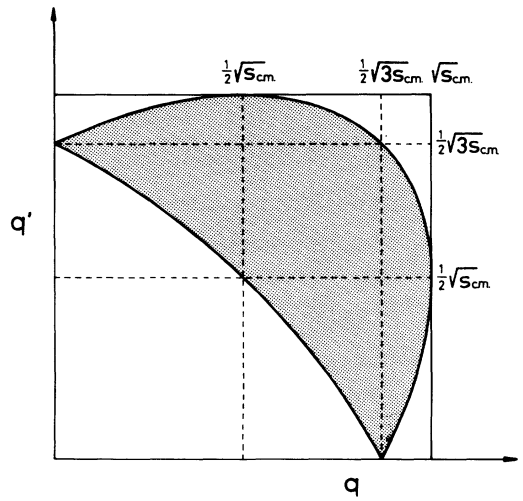

FIG. 17. Three-particle threshold curve. The interior sector is the three-particle scattering region.

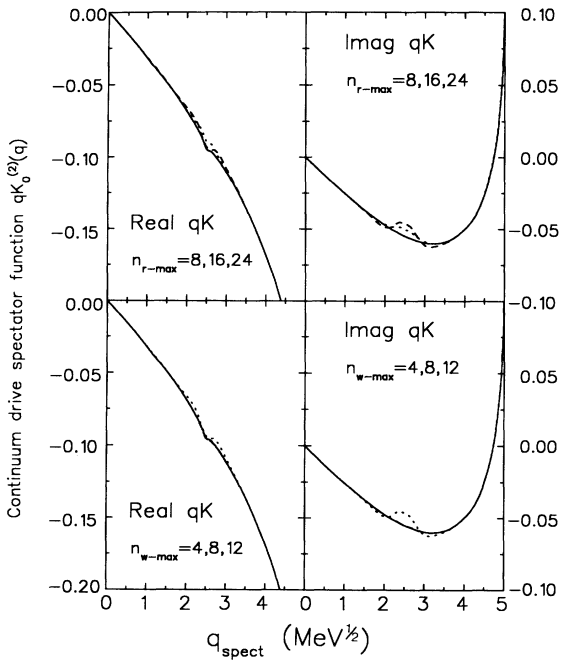

FIG. 18. Driving term $\psi_{l=0}^{(2)} = -8\pi K_{l=0}^{(2)}$ determined for an energy $s_{\text{c.m.}} = 25$ MeV and spectator momentum $q_f = 2.375$ MeV$^{1/2}$. The function $q\psi$ is actually plotted. The solid line corresponds to calculations with n_{reg} and n_ω set to their maximum values, while the dotted curves indicate the results for variations of n_{reg} (lower curves) or n_ω (upper curves).

$4 \leq n_\omega \leq n_{\omega_{\max}}$. The value $n_{\omega_{\max}} = 12$ turns out to be a good choice. $K_l^{(2)}(q_i\beta_i|q_f\beta_f)$ is calculated as a function of q_i for a fixed value of q_f. In arranging the grid of q_i values the spectator momentum q_f and the corresponding branch points $q_{\omega_{1_f}}$ and $q_{\omega_{2_f}}$ serve as a guide. Coincidences are avoided such that the above scheme can be employed without modifications. If $q_i^2 > s_{\text{c.m.}}$ a situation similar to the N-d breakup process is recovered.

To study the sensitivity on the values for $n_{\text{reg}_{\max}}$ and $n_{\omega_{\max}}$ we have plotted the $\psi_{l=0}^{(2)}$ function at an energy $s_{\text{c.m.}} = 25$ MeV and a spectator momentum $q_f = 2.375$ MeV$^{1/2}$. The result is shown in Fig. 18.

Clearly visible is the cusplike structure at q_f and $q_{\omega_{1_f}} = 2.623$ MeV$^{1/2}$. In general the $q_{\omega_{2_f}}$ point is too close to the $\sqrt{s_{\text{c.m.}}}$ boundary where the threshold behavior dominates, so that no cusp structure is seen in that case. The discussed cusp structures arise from the onset of the overlap of the three-particle sectors $[q_{\omega_{1_i}}, q_{\omega_{2_i}}]$ and $[q_{\omega_{1_f}}, q_{\omega_{2_f}}]$. For example, the pure residue contribution

$$-\sum_\beta \int dq\, I_l(q_i\beta_i|q\beta)\tau(s-q^2;\beta)I_l(q\beta|q_f\beta_f)$$

exhibits such a structure as a function of q_i at fixed q_f. As is shown in Fig. 18 the region around the final spectator momentum and its branch points requires a very detailed numerical analysis. But even then some numerical error remains present due to the discretization. However, we found that this inaccuracy does not seriously affect the calculated values of the scattering series. Based on this we decided to use the $K_l^{(2)}$ contribution as the driving term for the subsequent iterations without taking any further precautions.

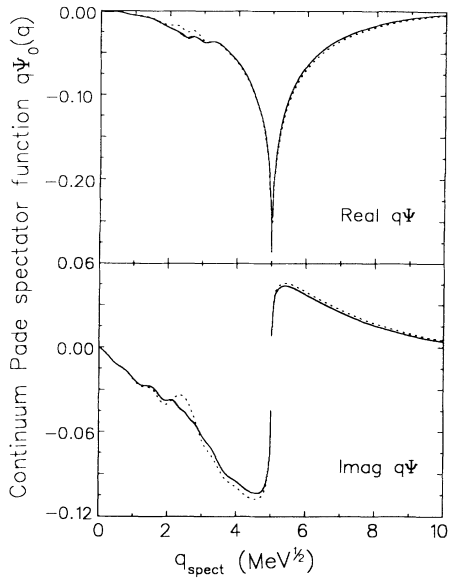

FIG. 19. Multiple scattering spectator function for $3N \to 3N$ scattering. The parameters correspond to the solid curves of Fig. 18.

The analysis of $B^{(2)}$ can be done in a slightly different way. In determining the principal-value contribution R_l [Eq. (C7)] the Legendre polynomial P_l can be combined with the subtraction function f [Eq. (C11)], i.e.,

$$R_l(q\beta|q'\beta') = \tfrac{1}{2}P\int_{-1}^{+1} dx \frac{P_l(x)f(x(q,q');\beta\beta') - \int_{-1}^{+1} dy\, P_l(y)f(y(q,q');\beta\beta')\delta(y-x_s)}{x-x_s}, \tag{C20}$$

such that the subtraction is confined to the three-particle sector. The residue contribution I_l in Eq. (C9) does not change, but the function W_l of Eq. (C8), which contains the logarithms, takes the form

$$W_l(q\beta|q'\beta') = -\int_{-1}^{+1} dy\, Q_0^P(y)P_l(y)f(y(q,q');\beta\beta')\delta(y-x_s)\,. \tag{C21}$$

An obvious advantage of this procedure is that W_l is only nonzero in the three-particle sectors $[q_{\omega_{1_i}}, q_{\omega_{2_i}}]$ and $[q_{\omega_{1_f}}, q_{\omega_{2_f}}]$. Consequently, the evaluation of the contribution in Eq. (C16) can be restricted to four subintervals in the integration scheme, which is shown before. In the calculation of the electromagnetic three-body breakup amplitude we have employed the separation of the kernel according to Eqs. (C20) and (C21).

Once the driving term for the continuum multiple scattering series is calculated we can proceed with the iterations of the multiple scattering series. The spectator function $\psi_l^{(2)}$ is obtained by multiplying $K_l^{(2)}$ with a factor -8π. The factor arises from the alternating character of the scattering series (-1), the number of diagrams involved in each next scattering (2), and the integration over a full solid angle (4π). The construction of the continuum spectator wave function $\Psi^{(\text{Padé})}$, which accounts for the complete multiple scattering series apart from the rescattering term $\Psi^{(1)}$, proceeds along exactly the same lines as in the N-d breakup analysis and without any modifications we can apply the already discussed method of Padé approximants. The structure of the three-nucleon wave function is equivalent to $B^{(1)}$ in Eq. (C2) and becomes

$$F(\mathbf{p}_1\mathbf{q}_1\beta_1|\mathbf{p}_f\mathbf{q}_f\beta_f) = \frac{1}{p_1^2+q_1^2-s_{\text{c.m.}}-i\varepsilon} g(p_1;\beta_1)\tau(s_{\text{c.m.}}-q_1^2;\beta_1)\Psi^{(\text{Padé})}(\mathbf{q}_1\beta_1|\mathbf{q}_f\beta_f)\tau(s_{\text{c.m.}}-q_f^2;\beta_f)g(p_f;\beta_f)\,. \tag{C22}$$

As an example we have plotted the multiple scattering spectator wave function (Fig. 19). The parameters $s_{\text{c.m.}}$ and q_f are the same as in Fig. 18.

As a final remark we note that the continuum wave functions carry the spectator momentum q_f as an extra parameter. At each energy we typically need 10–15 values for q_f. Together with the high accuracy determination of the second rescattering term, the required CPU time increases by about a factor of 50 as compared to multiple scattering with a N-d physical state.

APPENDIX D: INTEGRATIONS OF THE SQUARED AMPLITUDE

A full treatment of the three-body breakup process requires the evaluation of the integrals in Eqs. (19) and (20), where the squared amplitude I is composed from all possible diagrammatic contributions to the amplitude M. To perform the integration accurately it is necessary to know more specifically the characteristic behavior of the function I of Eq. (13). The integration procedure explained hereafter is valid for the case of nonrelativistic kinematics, but a similar prescription is obtained for relativistic kinematics.

The integration over the pair momentum $\mathbf{p}_f$ yields the nuclear structure functions W in Eq. (19). The radial integration trivially removes the energy conserving delta function present in I giving rise to a nonrelativistic phase space factor $\frac{1}{2}\sqrt{s_{\text{c.m.}}-q_f^2}$. The generally weak dependence on the azimuthal angle ϕ_{p_f} is purely due to exchange contributions. These are represented by the $n=2$ and $n=3$ terms in the various amplitudes of Eqs. (32), (33), and (35). To obtain numerically equal results for the $n=2$ and $n=3$ terms separately (apart from the overlap), the integration interval $[0,2\pi]$ is divided into two subintervals $[0,\pi]$ and $[\pi,2\pi]$. A Gauss-Legendre quadrature with $n_{\phi_{p_f}}=3$ points in each subinterval already leads to an accurate result.

The integration over the polar angle θ_{p_f} requires a more detailed examination. As we have seen before the trinucleon spectral function shows a pronounced maximum at missing energy $E_m=0$ and missing momentum $q_m=0$. In PWIA-type diagrams the values of the integration variables at these points are given by

$$p_f^2=0\ ,\qquad \mathbf{q}_f=-\mathbf{Q}_m=-\mathbf{Q}/\sqrt{3M_N}\ . \tag{D1}$$

However, these relations are valid for the associated momentum $\mathbf{p}_{f_n},\mathbf{q}_{f_n}$ $(n=2,3)$ as well. In terms of the integration momenta, significant contributions to the nuclear structure functions, which correspond to the exchange contribution $n=2$ and $n=3$, will show up at

$$\begin{aligned}0\approx E_m=p_{f_n}^2&=\tfrac{1}{4}p_f^2+\tfrac{3}{4}q_f^2\mp\tfrac{1}{2}\sqrt{3}\,\mathbf{p}_f\cdot\mathbf{q}_f\ ,\\ 0\approx\mathbf{q}_m^2&=\tfrac{3}{4}p_f^2+\tfrac{1}{4}q_f^2+Q_m^2\mp\sqrt{3}\,\mathbf{p}_f\cdot\mathbf{Q}_m-\mathbf{q}_f\cdot\mathbf{Q}_m\\ &\quad\pm\tfrac{1}{2}\sqrt{3}\,\mathbf{p}_f\cdot\mathbf{q}_f\ .\end{aligned} \tag{D2}$$

The second condition, $\mathbf{q}_m^2=0$, can only be fulfilled at the quasielastic peak, $s_{\text{c.m.}}=Q_m^2$. At this point the combination of values

$$\begin{aligned}&p_f^2=\tfrac{3}{4}s_{\text{c.m.}}\ ,\quad y_f=\hat{\mathbf{p}}_f\cdot\mathbf{Q}_m=\pm1\ ,\\ &q_f^2=\tfrac{1}{4}s_{\text{c.m.}}\ ,\quad x_f=\hat{\mathbf{q}}_f\cdot\mathbf{Q}_m=+1\ ,\end{aligned} \tag{D3}$$

completely satisfies the conditions in Eq. (D2). Off the quasielastic peak we relax the second condition of Eq. (D2) and search for the lowest possible value of $\mathbf{q}_m^2$. In that case the phase space values in Eq. (D3) again define the region with the largest contributions, but the maxima are less pronounced. [In Eqs. (D2) and (D3) the upper (lower) sign corresponds to $n=2(3)$.] This analysis implies that the integrand I will be peaked at forward or backward angles θ_{p_f}, which is confirmed by numerical investigation. Moreover, this type of behavior is present in almost the entire phase space region, although the function I is much smoother outside the quasielastic points. To account accurately for the polar integral with a reasonable number of mesh points the integration variable is casted into a form which samples the forward and backward angles more effectively. For this we used the substitution

$$y_{p_f}\rightarrow\tilde{y}_{p_f}=\sin\frac{\pi}{2}y_{p_f}\ . \tag{D4}$$

This mapping gives surprisingly fast converging results. Already $n_{\tilde{y}_{p_f}}=8$ is sufficient, provided that I behaves as discussed above.

A subsequent integration over the spectator momentum $\mathbf{q}_f$ yields the response functions according to Eq. (20). As is already pointed out, the azimuthal integration removes the contribution from W_I, whereas W_T and W_S contribute to the inclusive cross section with the same transverse electron-photon factor [Eq. (7)]. The x_{q_f} dependence of W appears to be quite similar to the y_{p_f} dependence of I and again we used the substitution of Eq. (D4) in order to perform the x_{q_f} integration. The radial integration is recasted into an integral over the missing energy $E_m=s_{\text{c.m.}}-q_f^2$. This integral is carried out keeping in mind the presence of pronounced maxima at $q_f^2\approx s_{\text{c.m.}}$ and $q_f^2\approx\frac{1}{4}s_{\text{c.m.}}$. Therefore the entire interval is subdivided into $[0,\frac{3}{4}s_{\text{c.m.}}]$ and $[\frac{3}{4}s_{\text{c.m.}},s_{\text{c.m.}}]$ and accurate integrations are performed with a 12–4 point Gauss-Legendre grid, once more using substitutions equivalent to Eq. (D4).

[1] K. Dow *et al.*, Phys. Rev. Lett. **61**, 1706 (1988); K. Dow, Ph.D. thesis, MIT, 1987.

[2] H. Meier-Hajduk, C. H. Hajduk, P. U. Sauer, and W. Theis, Nucl. Phys. **A395**, 332 (1983).

[3] C. Ciofi degli Atti, E. Pace, and G. Salme, Phys. Lett. **127B**, 303 (1983).

[4] E. van Meijgaard and J. A. Tjon, Phys. Rev. C **42**, 74 (1990).

[5] E. van Meijgaard and J. A. Tjon, Phys. Rev. C **42**, 96 (1990).
[6] R. A. Malfliet and J. A. Tjon, Nucl. Phys. **A127**, 161 (1969); Ann. Phys. (N.Y.) **61**, 425 (1970).
[7] E. Harms, Phys. Rev. C **1**, 1667 (1970); E. Harms and V. Newton, *ibid.* **2**, 1214 (1970).
[8] E. Jans *et al.,* Nucl. Phys. **A475**, 687 (1987).
[9] C. Marchand *et al.,* Phys. Rev. Lett. **60**, 1703 (1988).
[10] T. de Forest, Jr., Nucl. Phys. **392**, 232 (1983).
[11] G. Höhler, E. Pietarinen, I. Sabba-Stefanescu, F. Borkowski, G. G. Simon, V. H. Walther, and R. D. Wendling, Nucl. Phys. **B114**, 505 (1976).
[12] E. van Meijgaard and J. A. Tjon, Phys. Lett. B **228**, 307 (1989).
[13] W. M. Kloet and J. A. Tjon, Ann. Phys. (N.Y.) **79**, 407 (1973).
[14] R. Schiavilla, V. R. Pandharipande, and R. B. Wiringa, Nucl. Phys. **A449**, 219 (1986).
[15] W. M. Kloet and J. A. Tjon, Nucl. Phys. **A210**, 380 (1973).
[16] A. R. Edmonds, *Angular Momentum in Quantum Mechanics* (Princeton University Press, Princeton, NJ, 1957).

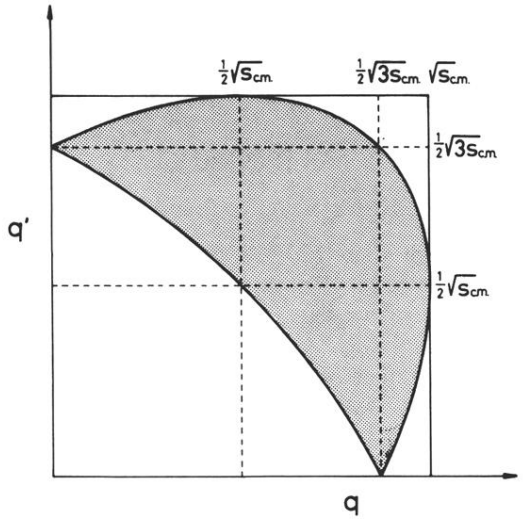

FIG. 17. Three-particle threshold curve. The interior sector is the three-particle scattering region.